2012

Observations and Analysis of Fire-Atmosphere Interactions during Fire Front Passage

Daisuke Seto
San Jose State University, daisuke.seto@sjsu.edu

OBSERVATIONS AND ANALYSIS OF FIRE-ATMOSPHERE INTERACTIONS DURING FIRE FRONT PASSAGE

A Thesis

Presented to

The Faculty of the Department of Meteorology and Climate Science

San José State University

In Partial Fulfillment

of the Requirements for the Degree

Master of Science

by

Daisuke Seto

August 2012

The Designated Thesis Committee Approves the Thesis Titled

OBSERVATIONS AND ANALYSIS OF FIRE-ATMOSPHERE INTERACTIONS DURING FIRE FRONT PASSAGE

by

Daisuke Seto

APPROVED FOR THE DEPARTMENT OF METEOROLOGY AND CLIMATE SCIENCE

SAN JOSÉ STATE UNIVERSITY

August 2012

Dr. Craig B. Clements (Chair)	Department of Meteorology and Climate Science
Dr. Sen Chiao	Department of Meteorology and Climate Science
Dr. Warren E. Heilman	USDA Forest Service

ABSTRACT

OBSERVATIONS AND ANALYSIS OF FIRE-ATMOSPHERE INTERACTIONS DURING FIRE FRONT PASSAGE

by Daisuke Seto

Wildfire responds to variations in fuels, topography, and weather. Wildfire frequency is expected to increase due to climate change, and fire management will become more important in the future. While numerical models are essential for predicting fire behavior and better simulations will improve fire fighter and public safety, there is a lack of observational data available for calibrating the model performances.

Four experimental studies were conducted with various types of vegetation fuel and terrain using in-situ instrumented towers to better understand fire-atmosphere interactions at both large and fine scales. The first part of the thesis focuses on a unique observation of fire whirl formation during a valley wind-sea breeze reversal. We hypothesized that the fire whirl was caused by the interaction of the vertical wind shear with the fire front, which resulted in vorticity estimate of 0.2 s^{-1} and turbulence kinetic energy of 10.4 $m^2 s^{-2}$. In the second part, turbulence generated by fire was investigated using spectral analysis to determine the role fire had on the energy spectrum of the wind and temperature. The results showed increased energy in velocity and temperature spectra at high frequency during fire front passage (FFP) for all four cases, but the spectral energy of velocity components at lower frequencies may be affected by cross-flow intensity, topography, presence of canopy layer, and degree of fire-atmosphere coupling. The velocity spectra observed during FFP collapsed into a narrow band at high frequency. The observed temperature spectra did not converge into a narrow range.

ACKNOWLEDGEMENTS

I would first like to thank my advisor Dr. Craig Clements for providing me opportunities to explore this field of research. After accompanying him on several field experiments I now have the knowledge to lead field experiments. I am also thankful for his strong scientific insight and high standards. Drs. Sen Chiao and Warren Heilman were essential in advising corrections to my writing and work, as well as guiding me through my data interpretation and analysis.

I like to thank Dr. Tara Strand for her guidance and support in the field during the sub-canopy transport and dispersion of smoke experiments. Xindi Bian is thanked for his help during the first phase of the turbulence spectra analysis.

I would like to thank past and present members of the Fire Weather Research Laboratory; particularly Fred Snively, Scott Strenfel, Kari Kiefer, and Allison Charland. Much of this work would not be possible without them. The entire student body and faculty in the Department of Meteorology at San José State University have made my experience unforgettable. The togetherness will be greatly missed.

Although far away, I would like to thank my family for their support and encouragement. This work was supported by a Joint Venture Research Agreement with USDA Northern Research Station grant # 07-JV-11242300-073. I was also supported with funding from Joint Fire Science Program. Lastly, I wish to thank the three anonymous reviewers whose comments greatly improved the manuscript that became Chapter 2.

TABLE OF CONTENTS

LIST OF FIGURES

LIST OF TABLES

CHAPTER 1

Introduction and Background

Wildfire is a physical process that responds to variations in fuels, topography, and weather. There is growing awareness of adverse effects of large, uncontrolled fires, as wildfires not only cause significant economic costs and loss to life annually but also influence ecosystem patterns and processes such as vegetation distribution and structure, the carbon cycle, and global climate (Bowman et al. 2009). Westerling et al. (2006) and Running (2006) show that increased large wildfire activity in the Western U. S. is associated with increased spring and summer temperatures and an earlier spring snowmelt. While wildfire management may become more important in the future as climate change modifies wildfire frequency, the fundamental role of fire-atmosphere interactions on fire behavior has not been fully understood.

The complex interactions of fuels, topography, and weather can occasionally result in extreme fire behavior. Extreme fire behavior defined by National Interagency Fire Center implies a level of fire characteristics that would make it difficult to control and involves one or more of the following: high rate of spread, prolific crowning and/or spotting, presence of fire whirls, and a strong convection column. Extreme fire behavior can result in compromised fire fighter safety and increased danger to communities. Recently re-defined critical weather elements that promote extreme fire behavior include low relative humidity, strong surface wind, unstable air, and drought (Werth 2011). The interaction of the fire with the atmosphere is highly nonlinear because fires influence the atmosphere by perturbing the ambient flow and injecting heat, whereas atmospheric

conditions influence fires because atmospheric wind, moisture, and temperature affect rates of fire spread.

When wildfires are driven by the wind (wind-driven fires), the fire is a two-dimensional, surface phenomenon, and thus the behavior and spread rate of the fire are predictable. When the hot gases rising above the fire produce a strong convection column under light wind conditions (convection-dominated fires), however, the fire needs to be considered as a three-dimensional phenomenon because the convection column can drive strong inflows and outflows on the surface. When the convection column drives its own wind circulation, the fire spreads independently of the ambient winds. Therefore, the convection-dominated fires make the fire spread far less predictable than for wind-driven fires. Additionally, convection-driven fires can produce pyrocumulus clouds atop the convection columns, which occasionally develop into cumulus congestus or cumulonimbus if the atmosphere is favorable for such deep moist convection (Banta et al. 1992).

The convective Froude number, F_c, is defined by the ratio of the kinetic energy of the air over the fire to the sensible heat flux provide by the fire (Jenkins et al. 2001). It is intended to help identify when a fire is dominated by convective forcing as opposed to being dominated by the energy of the ambient wind field. The convective Froude number, similar to Byram's energy criterion (Byram 1959), was introduced by Clark et al. (1996a) as a controlling parameter in simulations of coupled forest fire and atmospheric dynamics, and the utility of F_c was assessed in Clark et al. (1996b). However, Sullivan (2007) recently re-examined the convective Froude number and

concluded that it did not reflect observed fire behavior. Kiefer (2009) also points out that dependence of the convective Froude number on poorly controlled variables such as perturbation of near-surface potential temperature limits the analysis of Clark et al. (1996a, 1996b).

Numerical models are essential for predicting fire behavior and spread rate, and better models will ultimately improve fire fighter and public safety. Although various models had been developed in the past to assist fire managers, most of the models treated the effect of fires on the atmosphere as an uncoupled system and no account was taken for direct interactions between the fire and atmosphere. However, significant progress in wildfire simulations has been made in recent years. For example, Clark et al. (1996a) coupled a fire model with a mesoscale atmospheric model in order to allow for two-way interaction between the fire and the atmosphere that occur over spatial scales from tens of meters or less to several kilometers or even larger. They successfully simulated a previously-observed "zigzag" fireline shape caused by convective-scale atmospheric motions. Since then, these types of numerical models, so-called coupled fire-atmospheric models, have become popular research tools and used by several investigators (i.e., Coen 2005; Dupuy et al. 2011; Filippi et al. 2011; Linn and Cunningham 2005; Linn et al. 2012; Sun et al. 2009). Although local- and fine-scale information on fuel, topography, and winds are essential for successful wildfire and fire spread models, knowledge of the small-scale atmospheric circulations in and around a wildfire is primary (Jenkins et al. 2001). Sun et al. (2009) used the coupled University of Utah's Large-scale Eddy Simulation (UU-LES) model to investigate the effects of fire-induced flow and

turbulence in the ABL on rate of grass fire spread. They found that a strong downdraft behind the head of the fire line, which results from an interaction between the fire-induced plume circulation and a strong eddy circulation in the ABL, is perhaps the main contributor to the enhanced fire-induced flow and the variability in fire spread rate and area burnt.

There have been various attempts to obtain realistic datasets that describe some qualitative and quantitative aspects of fire behavior. Banta et al. (1992) utilized Doppler radar and lidar to demonstrate the usefulness of remote-sensing techniques in observing three-dimensional kinematic quantities of convection column and smoke plume during forest fires. Clark et al. (1999) applied an IR video camera and image flow analyses to derive high resolution wind fields and sensible heat flux during an intense crown fire. While the IR video camera imagery analysis allows for much finer temporal and spatial resolutions than scanning radar or lidar can, Clark et al. pointed out that it also requires further evaluation and validation. IR video camera imagery has also been used to identify flame geometry (Butler et al. 2004; Morandini et al. 2006). Both remote sensing systems can provide valuable data of fire behavior necessary for developing realistic forest and grass fire models. In addition, in-situ measurements have been recently conducted in order to obtain comprehensive datasets for model validation. Those include measurements of water vapor, heat, and carbon dioxide fluxes (Clements et al. 2006), mean and turbulent flows, the plume dynamics, and fire-atmosphere interactions (Clements et al. 2007; Clements et al. 2008), and thermodynamic structure of the smoke plume (Clements 2010) associated with wildland grass fires. Plume temperatures and

heat fluxes were measured in Mediterranean shrub (Morandini and Silvani 2010; Morandini et al. 2006; Santoni et al. 2006; Silvani and Morandini 2009) and in boreal forest (Butler et al. 2004; Cohen 2004). As Clements et al. (2008) successfully captured fire-induced circulations that were also numerically shown by Sun et al. (2009), in-situ platform measurements provide some viable data necessary for physical guidance and the validation of coupled fire-atmosphere models.

To gain a better understanding of the dynamics of fire-atmosphere interactions that occur during wildfires, four field experiments were conducted. Fine temporal resolution of wind, temperature, and several other variables were measured. This thesis is organized into sections describing observations and analysis of fire-atmosphere interactions. In Chapter 2, unique observations made of the evolution of a small fire whirl that formed during a prescribed grass fire conducted in a narrow mountain valley are presented. The meteorological conditions and heat release measured at a tower located in the vicinity of the fire were examined in an attempt to determine what caused the observed fire whirl to form. A preliminary analysis of the turbulence spectra measured as a fire front passed through an in-situ micrometeorological tower during the four field experiments conducted under various terrain and atmospheric conditions are presented in Chapter 3. A summary of the thesis is presented in Chapter 4 with some discussion of future work.

CHAPTER 2

Fire behavior observed during a valley wind-sea breeze reversal

Adapted from: Seto and Clements, 2011: Fire Whirl Evolution Observed during Valley Wind-Sea Breeze Reversal. *Journal of Combustion* (doi:10.1155/2011/569475)

Abstract

This observational study documented the atmospheric environment of a prescribed fire conducted in a narrow valley when a small fire whirl developed during a mesoscale wind reversal. Based on analysis of in situ meteorological measurements, it is hypothesized that the fire whirl formed due to the presence of strong vertical wind shear caused by the interaction of a sea breeze front with a weaker up-valley wind. Vorticity generated by the interaction of the wind shear and the fire front was estimated to be ~0.2 s^{-1}. Peak turbulence kinetic energy was caused by the wind shear rather than the buoyancy generated by the fire front. It was also found that the convective Froude number itself may not be sufficient for fire whirl prediction since it is less relevant to the near-surface boundary-layer turbulence generated by environmental wind shear. Observations from this case study indicate that even low-intensity prescribed fires can result in the formation of fire whirls due to mesoscale changes in the ambient atmospheric environment.

2.1 Introduction

Wildland fire is a physical process that responds to variations in fuels, topography, and weather. The complex interactions between these can occasionally

result in extreme fire behavior. Extreme fire behavior defined by National Interagency Fire Center implies a level of fire behavior characteristics that would make a fire difficult to control and involves one or more of the following: high rate of spread, prolific crowning and/or spotting, presence of fire whirls, and a strong convection column. Extreme fire behavior can result in compromised fire fighter safety and increased danger to communities. One of the fascinating phenomena of extreme fire behavior is fire whirls. Forthofer et al. (2009) define fire whirls as vertically oriented, rotating columns of air found in or near fires. Fire whirls are often associated with extreme meteorological conditions and fire-atmosphere interactions. Fire whirls can transport fire far beyond the fire front, and they can also spread flames vertically. Graham (1952) observed a fire whirl that became violent enough to break off trees at their bases.

Several environmental factors impact the formation of fire whirls including vorticity, atmospheric stability, and topography. Environmental vorticity can be produced in the atmosphere by vertical wind shear forming eddies and rotation of the surface air (Countryman 1971). Umscheid et al. (2006) observed and photographed a large fire whirl that lasted for about 20 min and occurred during a slow moving cold front where pre-existing environmental vertical vorticity interacted with a wheat stubble field burn causing the fire whirl development.

Atmospheric instability is a favorable condition for fire whirl development because strong updrafts produced by an unstable atmosphere itself can start fire whirls (Countryman 1971). However, Byram (1954) points out that it is an entirely normal condition for large fires to cause warmer air below cooler air and fire whirls are only

present where the atmosphere is in particular unstable conditions; therefore, there must be some conditions other than instability by heating to cause their formation.

First, fires on steep lee slopes present a favorable situation for fire whirls to develop (Countryman 1971; Forthofer et al. 2009). For example, Graham (1957) observed 28 fire whirls that formed in mountainous terrain and reported that 20 of the fire whirls formed on lee slopes. The ridge acts as an obstruction to airflow, causing mechanically induced eddies on the lee side. The lee side of the slope is an ideal location for the convergence of the upslope flow of hot gases and the cool opposing ambient wind crossing the ridge potentially leading to strong wind shear. An observation of a destructive fire whirl by Pirsko et al. (1965) suggests that channeled drainage flows in steep canyons are conductive to turbulent winds. Forthofer et al. (2009) also suggested flow channeling in complex terrain as a potential source of vorticity. The topographic effects on the fire whirl formation are often mentioned as a primary cause of fire whirls (Graham 1957; Haines and Lyon 1990).

Second, a concentrating mechanism has been suggested in previous studies as a source of fire whirl formation (Countryman 1971; Forthofer et al. 2009; Heilman 1994; Meroney 2003). Buoyancy generated by the fire acts to converge nearby ambient eddies and vorticity, triggering the fire whirl formation. Tilting and stretching of horizontal vorticity most likely occurs above the flaming front, because hot gasses from the fire generate strong buoyant forcing. Occasionally, fire whirls are observed downstream of fire plumes as depicted by Fric and Roshko (1994). Clark et al. (1996) describe the formation of a near-surface convergence zone ahead of the fire line as a result of the

hydrostatic pressure gradient caused by the tilted plume and air being drawn into the convection column. The existence of the downwind convergence zone was verified by Clements et al. (2007) who measured the weak convergence of winds ahead of the fire front using in-situ tower measurements during an intense grass fire that generated a large fire whirl downstream of the fire front (Clements et al. 2008). Additionally, Hanley et al. (2005) found that the arrival of a sea breeze front during a wildfire resulted in a temporary increase in fire intensity as a result of enhanced convergence and vertical motion which could potentially lead to fire whirl formation.

There appears to be similarity in the conditions in which fire whirls and dust devils form, such as atmospheric instability and low-level wind shear. Smaller fire whirls are also comparable in size to dust devils that typically range from 6- to 60-m in diameter (Williams 1948). Bluestein et al. (2004) used a Doppler radar to measure the vorticity in a dust devil core. They showed the measured vorticity was similar to that in some tornadoes, but the maximum wind velocity of the dust devils was much weaker. The main difference between fire whirls and dust devils are that fire whirls maintain the rotating column from buoyancy generated by the combustion of the fire, whereas dust devils rely on the intense surface heating from insolation as a source of potential energy.

While fire whirls have been observed during a number of wildland fires, few observational studies have succeeded in measuring both the in-situ atmospheric environment and fire behavior simultaneously, thus the understanding of their dynamics is not well understood. In this paper, observations made during the interaction of a valley wind reversal and grass fire are explored to investigate the causes of fire whirl formation.

In addition, the convective Froude number, ambient turbulence kinetic energy, and resulting fire behavior are analyzed and compared with previous studies.

2.2 Experimental Design

2.2.1 Site description

The observational campaign was conducted during a vegetation management fire (prescribed burn) conducted by Cal Fire (California Department of Forestry and Fire Protection) on 7 October 2008 at Joseph D. Grant County Park. The park is located in the Diablo Range approximately 6.5 km east of San José, California and 60 km east of the Pacific Ocean (Fig. 1). The experimental site is located in the northwest-southeast oriented Hall's Valley, with a valley bottom elevation of 440 m MSL surrounded by ridges that rise 660 m on the west and 830 m on the east (Fig. 2). The burn unit was 0.14 km^2 (35 acres) in size, with fuels dominated by a mixture of grasses including Italian Rye (*Lolium Multiflotun*), Oat Grass (*Avena Barbartum*), Soft Brome (*Bromus Hordeaceus*) and Purple Needle Grass (*Nassella Pulchra*). The soils were dry and fuels were fully cured. The estimated fuel loading was 0.12 kg m^{-2} (0.5 tons $acre^{-1}$).

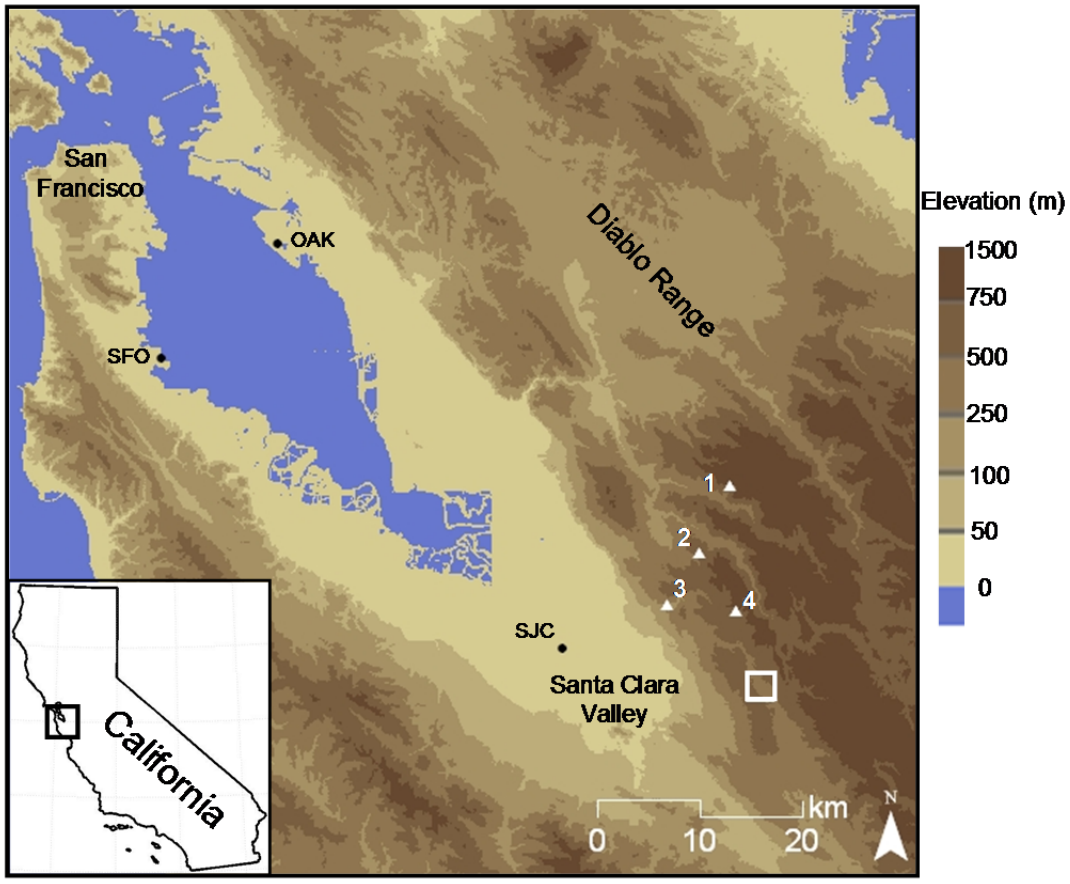

Figure 1. A map of San Francisco Bay Area indicating the geographical locations of Joseph D. Grant County Park (white box), and four nearby RAWS stations (1: Rose Peak (RSPC1), 2: Poverty (MIPC), 3: Alum Rock (RJSC1), and 4: CDF portable 10 (TR098)). Elevation above mean sea level (MSL) is shaded according to the scale. The inset map shows map location relative to California.

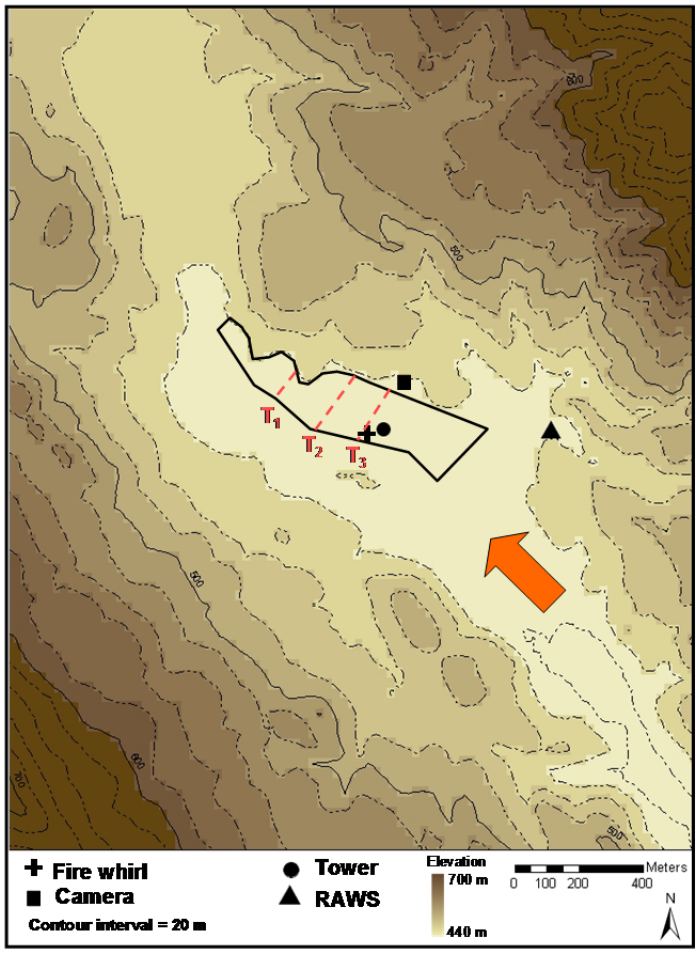

Figure 2. Contour map of the experiment site indicating instrument locations. The burn unit is indicated by the solid black line. The solid arrow indicates initial wind direction prior to the wind shift. The dashed red lines indicate approximate positions of the fire front: T1 = 11:45, T2 = 12:30, and T3 = 12:43.

2.2.2 Background meteorology

The synoptic conditions on the day of the prescribed burn were warm and dry under the influence of a building high-pressure ridge over the eastern Pacific and a weak thermal trough in place over central California. A shallow layer of stratus confined to Santa Clara Valley below the ridge crests was observed early in the morning, but the stratus did not fill into the Hall's Valley site the previous night due to the topographic

blocking. Nearby Remote Automated Weather Station (RAWS) temperature data supports that the cool marine air remained below 500 m MSL as indicated from the surrounding RAWS stations (Fig. 3). For example, at the elevation of 223 m MSL the Alum Rock site was influenced by the marine layer, while the other nearby RAWS stations at elevations above 500 m MSL remained above the marine inversion overnight (Fig. 3). The Oakland 12Z sounding (not shown), which is located 60 km north of site, also showed a moist surface layer below 500 m MSL along with weak northeast winds near the surface, indicating that the marine layer was below the ridge height and had not pushed further inland.

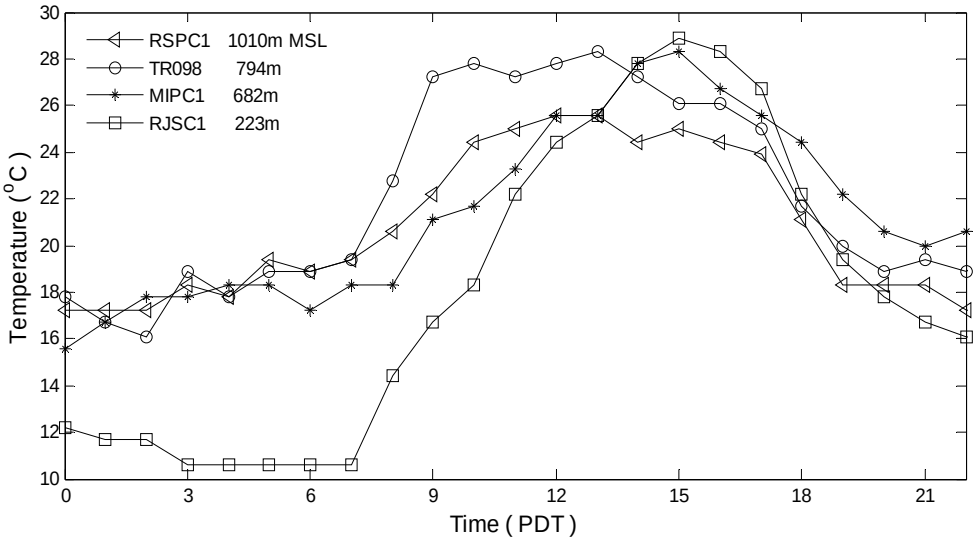

Figure 3. Time series of 60-min average temperatures recorded at nearby RAWS sites during the day of the burn. The relative locations of the RAWS stations are shown in Fig. 1.

In order to determine the ambient atmospheric stability and vertical wind profile at the valley site, a rawinsonde sounding was conducted on the valley floor ~1 km north northwest of the burn unit, at 0800 PDT (Pacific Daylight time). A shallow inversion

layer near the surface to 500 m AGL is evident from the temperature profile (Fig. 4a), and north to northeast winds within the layer are likely to be a combination of nocturnal down-valley and downslope winds (Fig. 4b). Very stable atmospheric conditions and a clear sky were evident throughout the lower troposphere as indicated by the sounding. However, the sounding does not represent the atmospheric environment during the ignition since the valley inversion broke before ignition

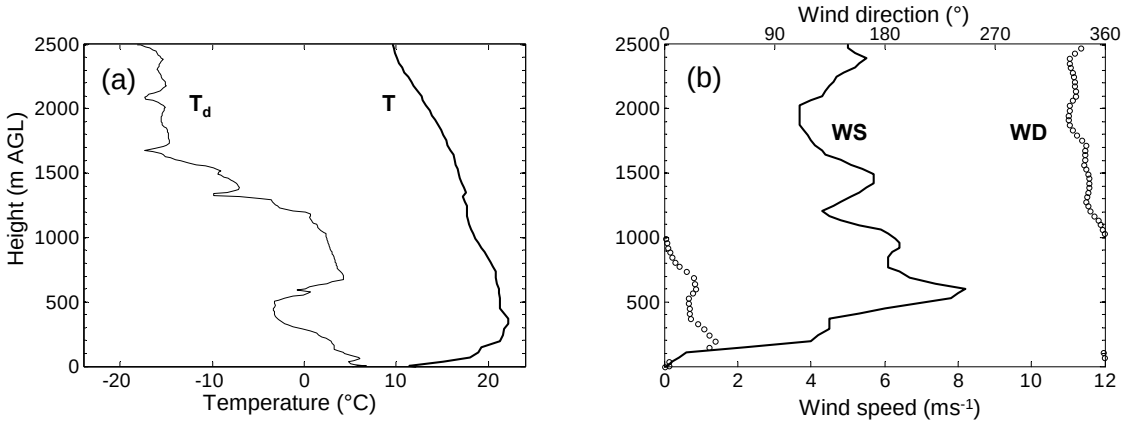

Figure 4. Vertical profiles of (a) air temperature T and dew point temperature T_d, and (b) wind speed (WS) and wind direction (WD) from radiosonde conducted ~1 km north northwest of the burn unit for the day of the burn, 7 October 2008 at 0800 PDT.

2.2.3 Instrumentation

The objective of the experiment was to capture and characterize fire-atmosphere interactions during a grass fire using high-frequency measurements. In order to capture the micrometeorology of the passing fire front, a 6.7-m guyed, steel tower was deployed near the center of the burn unit and the fire front was allowed to burn directly beneath it (Fig. 2). Fuels were removed 1.5 m from around the base of the tower in order to protect it from direct flame. The tower was equipped with a 3-D sonic anemometer (Applied Technologies, Inc., Sx-probe) mounted to the tower at 6-m AGL, four type-T

thermocouples (Omega, Inc. 5SC-TT-40) mounted at 0.15, 2, 2.7, and 3.5 m AGL, and a temperature and humidity sensor (Vaisala Inc. HMP45C) mounted at 2.5 m AGL. The sonic anemometer was sampled at 10 Hz while the thermocouples and temperature and humidity probe were sampled at 1 Hz. Additionally, total heat flux emitted from the fire front was measured with a Schmidt-Boelter heat flux sensor (Hukseflux, SBG01) that was attached to a cross arm mounted on the tower at 5 m AGL and extending 1.5 m away from the tower horizontally. The sensor transducer was pointed down at a 45° angle and outward towards the approaching fire front. The SBG01 was sampled at 10 Hz. In order to determine the time the plume impinged on the tower and instrumentation, the concentration of CO_2 in the smoke was sampled using a Vaisala Inc. GMP343 NDIR probe sampled at 1 Hz. All tower data were recorded using a Campbell Scientific, Inc. (CSI) CR3000 datalogger mounted near the base of the tower housed in an environmental enclosure. Additionally, the datalogger and the base of the tower were protected from the intense heat generated by the fire using fireproof insulation wrapped around the lowest 2 m of the tower.

To document the atmospheric conditions occurring outside of the burn unit, a portable weather station was located downwind and approximately 150 m away from the southeast corner of the burn unit (Fig. 2). A 3-m tripod was outfitted with a temperature and humidity probe (CSI, CS215), barometer (Vaisala Inc., PTB110), and a prop-vane anemometer (R.M. Young, 5103), all sampled at 1 Hz and stored as 1-min averages using a CSI CR1000 datalogger. There was 2-3 m tall brush surrounding the site, making the downwind weather station site slightly less exposed to the ambient wind than the interior

tower site. Fire behavior including spread rate and evolution of the fire front was documented using a digital SLR camera (Canon, Inc. 40D) with a 1 Hz time lapse function. The camera clock was synchronized to the datalogger clocks so that the time lapse photography could be compared to the time series data for analysis.

2.2.4 Burn operations and fireline evolution

The goal of the prescribed fire was the eradication of invasive grass species; however, the site was populated with native oak species requiring low-intensity backing fires (fire moving opposite the wind direction) to be used in order to limit scorching of the oaks. The experimental plan was to take advantage of the burn operations and measure fire-atmosphere interactions during the grass fire. One specific goal was to determine the role of fine-scale fire-atmosphere interactions on fire behavior during the passage of a head fire (fire that propagates with the ambient wind) which required the burn crew to ignite a single line, head fire upwind of the instrument tower.

During the initial back burning the wind was from the southeast, as an up-valley wind (Fig. 5), so the back burning began on the northern edge of the burn plot (Fig. 2: T_1, T_2). Once the back burning was completed, the burn crew began walking around the instrument tower to start a line ignition 100 m upwind (to the south) of the tower that would spread with the southerly wind and pass through the tower as a head fire. At this point (12:43 PDT) a 180º wind shift occurred at the surface and the initial backing fire began to run as a head fire towards the tower (Fig. 2, T_3). It was at this time that a fire whirl formed.

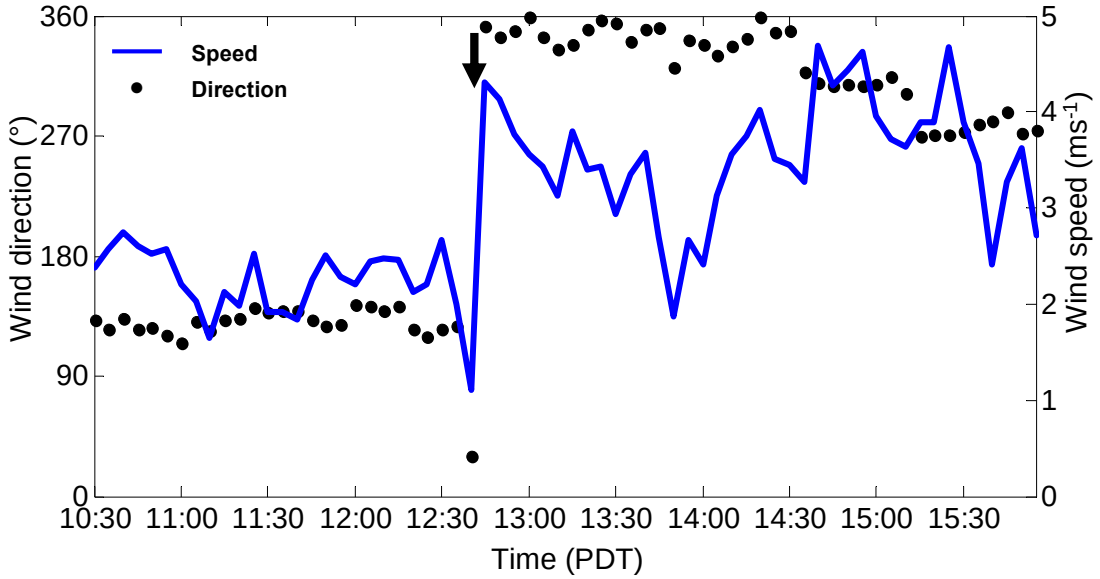

Figure 5. Time series of 5-min averaged wind speed and direction at the interior tower. Timing of fire whirl is indicated with solid arrow.

2.2.5 Evolution of wind reversal

The time series of 5-min average wind speed and direction from the interior tower (Fig. 5) shows that weak (< 3 m s^{-1}) south and southeasterly winds prevailed in the valley and were the daytime up-valley winds that typically occur in mountain valleys (Whiteman 1990; Rampanelli et al. 2004). By 12:45 PDT, the up-valley winds were replaced by a break-in of moderate (2.0 to 4.5 m s^{-1}) north to northwesterly flows associated with the sea breeze surge.

The evolution of the surface environment as the sea breeze arrived, as well as the timing of the fire whirl formation and dissipation, is shown in Fig. 5. Prior to the fire whirl formation (12:42 PDT), a southerly component of the wind (135 – 225°) was observed at the tower location. The sea breeze arrival is indicated by the shift in wind direction and the increase in relative humidity at 12:43 PDT. It is interesting to point out

that the first sign of the north-northwest winds that dominate the valley afterward are apparent as the fire whirl dissipates, as if the intensifying northerly winds act as the cutoff source of the fire whirl. The in situ measured data reveal that a much more complicated flow pattern occurred in front of the fire line during the transition period. This is discussed further in the following sections.

2.3 Results and Discussion

2.3.1 Fire whirl evolution

The fire whirl was observed approximately 35-m west of the interior tower (Fig. 2) during the period when the winds shifted from southerly to northerly. The time lapse photos and recorded video images were visually analyzed, and they show that the cyclonically rotating fire whirl formed at one end of the flaming front where the most intense flame was present at that moment. Countryman (1971) had previously noted that fire whirls form near the more intense region of the fire front.

Figure 6 shows a time series of photos taken during the entire evolution of the fire whirl from its initial formation to dissipation. A ~1 m wide, vertically rotating column of flame appeared within the fire front at 12:43:10 PDT (Fig. 6a). We inferred from the sequence of the time lapse photos between Fig. 6a and 6b (not shown) that the vorticity was already present within the flame by this time. The rotating column kept drawing the flame along the fire line into the base of the column (Fig. 6b) while the flame height at this time reached ~4 m AGL within the rotating column (Fig. 6c) before the flame disappeared altogether from the base of the fire whirl. This may have occurred

because the near-surface flow converged parallel to the fire front and toward the base of the fire whirl (documented in the sequence of the photos as well as in video), limiting the ignition of the unburned fuel ahead of the fire front and the forward spread of the fire. Therefore, the flame was no longer supplied to the base of the fire whirl. Although the rotating column of smoke initially appeared within the fire line, the fully formed fire whirl was observed to move backward into the black area behind the fire front (Fig. 6d). The fire whirl was still intensifying over the freshly burnt area (Fig. 6e) behind the fire line without any active combustion indicating that the hot ground can provide a source of energy for its further development. A maximum vertical extent of approximately 200 m AGL was observed (Fig. 7) once the fire whirl was fully formed (Figs. 6e and 6f).

Figure 6. Time-lapse photographs of the fire whirl evolution during a valley wind –sea breeze reversal. Times are indicated in the bottom of each panel in PDT.

Figure 7. Photograph of dissipating fire whirl near the surface while rotating column is still active aloft (1244 PDT). Tower can be seen in the bottom of the photograph.

A time series of the vertical velocity (Fig. 8b) shows a positive velocity peak at 12:43:38 PDT, followed by negative vertical velocity lasting until 12:44:00 PDT. It is interesting to note that the timing of the downward motion observed at the tower occurred at the time the fire whirl dissipated. Because the tower was located 35 m away from the fire whirl, it cannot be assumed the observed vertical velocity field is related to the evolution of the fire whirl. The horizontal wind speed also dropped to 0.4 m s^{-1} at this time (Fig. 9a) indicating a transition period from one wind regime to another and a brief period of convergence. It was also observed that the fire whirl dissipated from its base (Figs. 6g and 7), while the rotation and smoke column was still present aloft (Fig. 7). After the fire whirl dissipated at 12:44:00 PDT (Fig. 6h), northerly flow observed at the tower started intensifying in velocity (Figs. 9a and 9b), indicating the full onset of the sea breeze penetrating through the valley. It was observed that the intensified flow began

driving the flaming front towards the tower as a head fire with a faster rate of spread. Time lapse photography indicated a forward-tilting flame front and smoke plume approaching the tower. Flame height increased as well with increasing ambient wind speed as compared with the flame height during the up-valley wind event. This dramatic change in fire behavior occurred over a period of only 2 min.

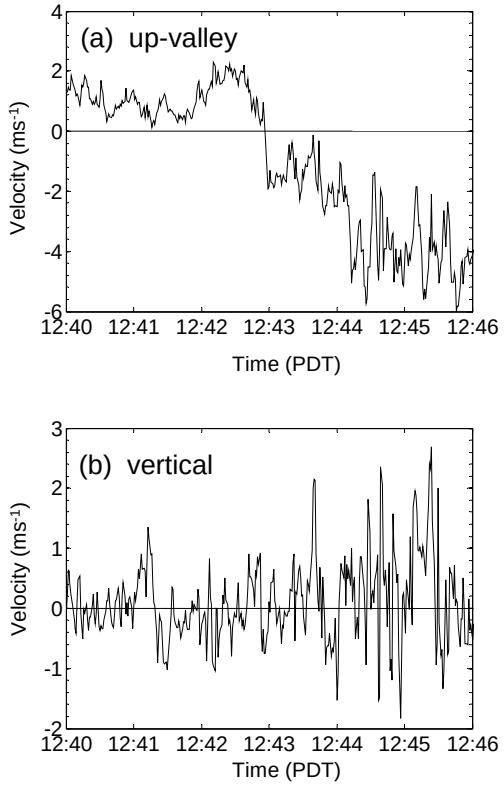

Figure 8. Time series of the 10-Hz wind velocities: (a) along-valley and (b) vertical velocity observed at the interior tower. Positive along-valley wind velocities in (a) indicate up-valley direction.

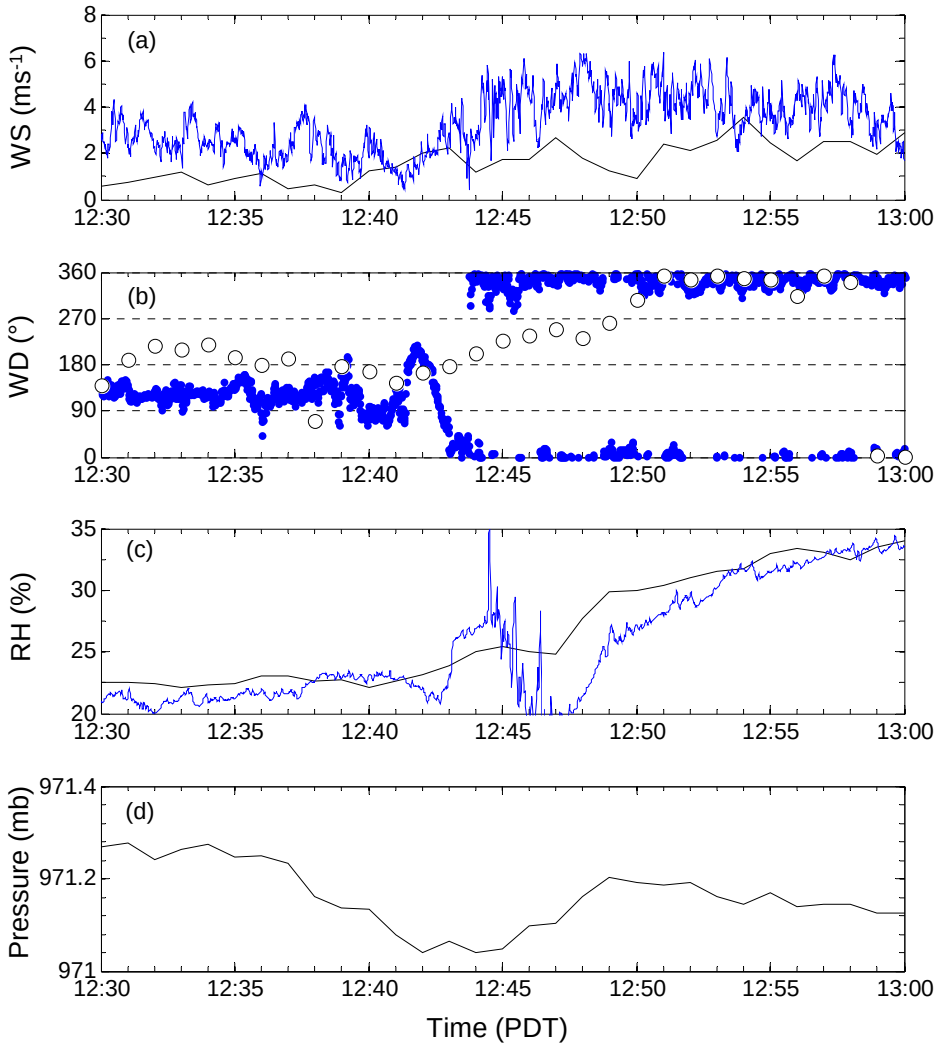

Figure 9. Time series of (a) wind speed, (b) wind direction, (c) relative humidity (RH), and (d) pressure measured at the interior tower and downwind RAWS between 12:30 and 13:00 PDT. The tower data and RAWS data are averaged over 1 s and 1 min, respectively. The blue represents the interior tower and the black represents the RAWS.

2.3.2 Evolution of the observed vorticity

The winds observed at the tower revealed a rather complex turbulence structure because of the presence of both the fire front and the interaction of the two opposing winds. Therefore, it only allows us to hypothesize what caused the vorticity formation in the valley. Over flat terrain, the leading edge of the sea breeze front is generally forced

upwards and backwards from the front by the opposing wind. It creates Kelvin-Helmholtz billows along its interface with the opposing ambient wind (Cunningham 2007; Simpson 1994). The vertical shear associated with opposing flows can produce the so-called hyperbolic wind profile (Clark et al. 1996) at low levels leading to the development of horizontal vorticity aligned perpendicular to the wind direction. When this type of wind shear interacts with a fire line, a pair of near-surface vortices may develop in front of the fire line and eventually touch down in the fire due to advection as described by Jenkins et al. (2001). The rotating vortices are caused by the tilting of the horizontal vorticity into the vertical by the updrafts associated with the fire front. Their simulations also show that a constant ambient wind profile can produce vortices but well in front of the fire line. The close proximity of the vortices to the fire line may play a critical role in the development of the fire whirl, such as in this case study, especially when fire is wind-driven and the surface wind drives the vortices well ahead of the fire line further downwind. In contrast, a moderate ambient wind decreasing slowly with height with weak vertical shear does not promote the extreme fire behavior as demonstrated by Jenkins et al. (2007).

Further analysis of the time-lapse photography shows that the rotating column of the fire whirl initially formed at the fire line and moved behind the fire line. This movement can be explained by the advection of vorticity due to the up-valley flow or by the development of a pressure perturbation/gradient that formed between the burnt area behind the fire front and the cooler air over the un-burnt area ahead of the fire front (Clark et al. 1996). In the photographs of Figs. 6b-6d the fire whirl jumped from the fire

line at 12:43:27 PDT (Fig. 6c) northwestward by approximately 6 m to a point estimated in Fig. 6d behind the fire line at 12:43:33 PDT. The wind direction at this time was 100° with velocities of 1.5-2 m s^{-1} (Figs. 9a and 9b) allowing the vorticity to advect over a period of 3-4 s.

Although the single-point-in-space tower measurements in this experiment do not directly provide enough parameters necessary to calculate the horizontal vorticity that is hypothesized to have formed at the fire line, it is possible to estimate the vorticity under several assumptions. The two-dimensional relative vorticity field ζ described by Heilman (1992) is defined as

$$\zeta = \frac{\partial w}{\partial y} - \frac{\partial v}{\partial z} \tag{1}$$

where w is the vertical velocity and v is the along-valley wind (sea breeze and up-valley wind) component that is perpendicular to the fire line. The instantaneous wind velocity components are shown between 12:40 and 12:46 PDT in Fig. 8. We determined $\partial w/\partial y$ from Eq. (1) by comparing the vertical velocity measured directly at the fire front and well before the fire front passage (FFP) occurred with a estimated distance of 10 m (between the fire front and the tower). The FFP is defined by Clements et al. (2008) as a maximum in the heat flux measured at the tower. It is the point where the fire front is closest to the tower as measured by the heat flux radiometers and peak in sensible heat flux from the sonic anemometers. The maximum observed vertical velocity associated

with the fire front (Fig. 8b) was ~2.8 m s^{-1} while the ambient vertical velocity measured was ~0.6 m s^{-1} resulting in an estimate for $\partial w/\partial y$ of ~0.22 s^{-1}. To determine $\partial v/\partial z$ we estimate that the depth of the sea breeze front to be ~200 m following observations by Simpson (1994). We determined the change in *v* using the observed averaged along-valley wind velocities (Fig. 8a). The up-valley wind of 1.1 m s^{-1} prior to the wind shift at 12:43 PDT and the sea breeze velocity of -3.4 m s^{-1} after the wind shift provide an estimated value of $\partial v/\partial z$ of 2.0×10^{-2} s^{-1} which agrees with the observed magnitude of the horizontal vorticity along a typical sea breeze front (Atkins et al. 1995). Therefore, the estimated ζ with the given assumptions in this case is approximately 0.2 s^{-1} which compares very well with the modeled vorticity (~0.2-0.3 s^{-1}) of Jenkins et al. (2007). This is most likely because the numerical set-up has several similarities with this field experiment such as grass fuels and the presence of environmental vertical wind shear. One major difference between the simulations and our experiment is that the simulation was made without a density current representing the sea breeze.

Based on the tower measurements, the sea breeze arrival is clearly evident by 12:43 PDT when the wind direction shifted to north and northeast (Fig. 9b) and the relative humidity (RH) sharply increased 5% over a 1-min period (Fig. 9c). Meteorological conditions were also measured at the downwind site (Fig. 2) on the portable RAWS station. Surface pressure at this site dropped ~0.2 mb at 12:38 PDT and recovered by 12:48 PDT (Fig. 9d). We speculate that the drop in pressure occurred not only at the RAWS site, but in the whole lower valley and is due to the development of a convergence zone that formed ahead of the sea breeze front as it entered the valley and

interacted with the opposing valley wind (Simpson 1994). At the same time the pressure recovery occurs, the wind direction shifted to a more northerly direction that we interpret as the dominant sea breeze direction in the valley. In addition, RH increased further, which indicates that the sea breeze front pushed further into the valley.

The transition between two wind regimes can lead to hazardous conditions for fire fighters due to the generation of unpredictable fire behavior. As observed in this case, the fire whirl appeared approximately 10 m away from the fire fighters (Fig. 6) and only 10 s after the wind reversal occurred. The video and time-lapse photos also showed fire fighters running away from the fire whirl indicating their sense of urgency and safety during this event. Although the period of interaction between the sea breeze front and the fire may be relatively short, the impact on fire behavior may be significant (Cunningham 2007; Hanley et al. 2005). Jenkins et al. (2007) point out that a background low-level vertical shear generated by a wind reversal with height is capable of generating extreme grassfire behavior and fire spread.

Furthermore, a fire whirl event was observed in a canyon of the Santa Ana Mountains by Schroeder (1961) who emphasized the potential for extreme fire behavior during a transition period between two wind regimes. Countryman (1964) found that certain geographic locations such as the lee side of ridge tops are favorable for two opposing currents to meet, and thus major fire whirl activity tends to occur frequently in these locations. Mountain valleys are a favorable location for the interaction of two wind regimes that differ in temperature and direction such as the wind reversal of valley winds (Whiteman 1990). It is likely that in this case the narrow Hall's Valley set up an

ideal environment for the interaction of the sea breeze and up-valley winds in the afternoon, as the elevated topography of the Diablo Range retarded the onset of the sea breeze preventing its penetration over the terrain until the up-valley flow was well established.

2.3.3 Turbulence characteristics

This section investigates the near-surface turbulence structure measured during the sea breeze break-in, the period associated with the fire whirl development, and the period the FFP occurred. One variable often used to quantify atmospheric turbulence is the turbulence kinetic energy (TKE). TKE is defined as the kinetic energy per unit mass associated with the amount of ambient wind shear present within an atmospheric layer (Heilman and Bian 2010). Following Stull (1988) the TKE is found by the sum of the velocity variances *u*, *v*, and *w*:

$$TKE = 0.5\left(\overline{u'^2} + \overline{v'^2} + \overline{w'^2}\right). \quad (2)$$

The variance of each wind velocity component is calculated from the processed 10 Hz sonic anemometer data which have been high-pass filtered to remove any spikes. Additionally, the time series of the velocity components has been tilt-corrected (Wilczak et al. 2001) in order rotate the components into the mean flow and remove any bias of the anemometer mounting not being precisely level during deployment. The turbulent components of the variables, u', v', w', T_s' are calculated by removing the mean from the instantaneous data. We have selected an averaging period of 10-min to calculate the

perturbations, while the averaging period chosen for the variance and TKE was 30 s which allowed the turbulent fluxes associated with the FFP and fire whirl to be isolated. Another key turbulent statistic is the sensible heat flux, $h_s = \rho c_p \overline{w'T_s'}$ where the term $\overline{w'T_s'}$ is the covariance between the vertical velocity perturbation and sonic temperature perturbation ρ is the density of air, and c_p is the heat capacity of air at constant pressure. The sensible heat flux was averaged over 1-min and allows us to also determine the timing of smoke plume and FFP at the tower.

Figure 10 shows a time series of the TKE and sensible heat flux (10a) and the individual velocity variances (10b-d). Although there is no increase in TKE between 12:43 and 12:44 PDT when the fire whirl was observed, a large increase in TKE is clearly evident prior to 12:43 PDT in Fig. 10a. The increase in TKE begins at 12:40 PDT with the value of 5.2 $m^2 s^{-2}$, compared to prior ambient background value of < 1.5 $m^2 s^{-2}$. The peak TKE occurs at 12:42 PDT with the value of 10.4 $m^2 s^{-2}$ before sharply dropping to 1.4 $m^2 s^{-2}$. It should be noted that the TKE started increasing three minutes before the relative humidity started increasing. We hypothesize that the interaction of the sea breeze front and up-valley flow started at 12:40 PDT, but the relative humidity increase was not detected by the humidity sensor due to the mixing of the air between the two flows. The second and third TKE peaks (5.0 and 4.5 $m^2 s^{-2}$) that occur at 12:45 and 12:47 PDT, respectively, are the turbulence associated with the FFP. Although the wind flow around the flaming area is known to be highly turbulent (Clements et al. 2008), observations indicate that the greatest TKE measured was caused by wind shear associated with the sea breeze arrival and is two times greater in magnitude than the TKE generated by the

passing fire front. The FFP is indicated by the maximum in sensible heat flux (~12.5 kW m^{-2}) that occurred at 12:45 PDT. The source of the turbulence kinetic energy generation is determined by diagnosing the velocity variances separately.

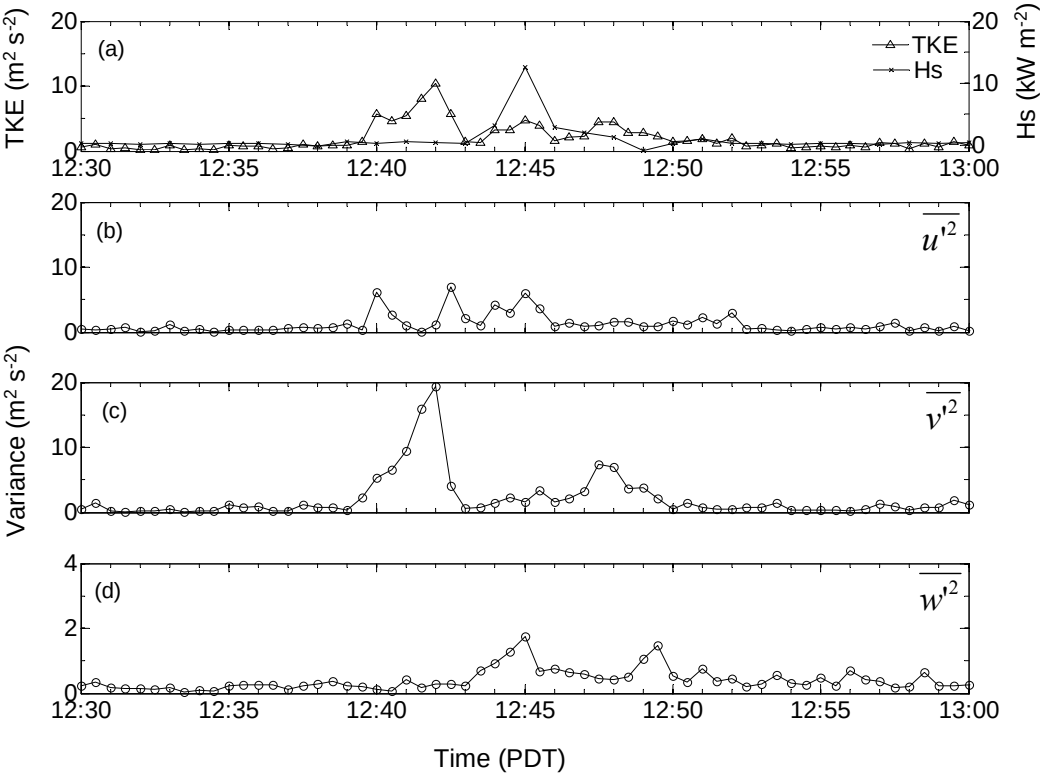

Figure 10. Time series of (a) 30-s averaged turbulence kinetic energy and 1-min averaged sensible heat flux, 30-s averaged *u* velocity variance (b), *v* velocity variance (c), and (d) *w* velocity variance.

The large increase in TKE between 12:40 to 12:43 PDT was dominated by $\overline{v'^2}$ which was nearly 20 $m^2 s^{-2}$ (Fig. 10c), while both $\overline{u'^2}$ and $\overline{w'^2}$ remained below 10 $m^2 s^{-2}$. Since the *v* variance represents north-south component of the turbulence intensity, it is most likely that the observed turbulence was caused by the wind shear generated between the southerly up-valley flow and northerly sea breeze. We also believe this shear to be responsible for setting up the horizontally rotating column of the air ahead of fire front

creating the observed vorticity and resulting fire whirl. The observed increase in $\overline{w'^2}$ at 12:45:00 (Fig. 10d) corresponds to the maximum in sensible heat flux. The second peak in $\overline{w'^2}$ (at 12:49:30 PDT) suggests an impact from smoldering after the FFP occurred. The maximum *w* variance of 1.5 $m^2 s^{-2}$ was much lower than the *v* component suggesting that wind shear played a larger role on the local turbulence than the sensible heat flux generated by the fire front. Comparing these results with other grass fire experiments (e.g., FireFlux: Clements et al. 2008) indicates that the values observed during this experiment are much lower than those reported by Clements et al. (2008) who measured peak *w* variances > 5 $m^2 s^{-2}$. This can be attributed to the fact that the heat flux observed during FireFlux was twice as large as observed in the present study. The reason for this can be simply due to a higher observed fuel loading measured during FireFlux (Clements et al. 2007).

2.3.4 Fire intensity

In previous studies, the fire intensity has been used primarily to determine resulting fire behavior. However, in order to determine the role the fire had on the development of the fire whirl, the heat release or fire intensity must be quantified. Byram (1954) and Graham (1957) associated fire whirl occurrence with large fire events or high intensity fires. Model simulations by Heilman and Fast (1992) also showed that the roll vortices become more vigorous with increased surface temperature. Although the tower was ~35 m away from the fire front when the fire whirl occurred, Taylor's assumption (Stull 1988) allows us to estimate the amount of heat supplied at the fire front to tilt the horizontally rotating column by assuming the heat flux measured at the tower at

(12:46:30 PDT) is the nearly the same during the fire whirl formation (12:43:10 PDT). A time series of the 1 Hz total heat flux (Hukseflux, SBG01 sensor) presented in Fig. 11a shows that the maximum in total heat flux of ~10 kW m^{-2} as the fire front approached and passed the tower. The instantaneous total heat flux of 12.3 kW m^{-2} (not shown) was nearly the same magnitude as the 1-min averaged sensible heat flux of 12.5 kW m^{-2} (Fig. 10a). We assume that the total heat flux present during the fire whirl formation is close to that measured at the tower given the uniform fuel type and flame lengths observed with the time-lapse camera. The total heat flux measured during the FFP of this particular grass fire was much lower compared to the radiant heat flux of 290 kW m^{-2} measured during a crown fire (Cohen 2004) and lower than the maximum total heat flux of 112 kW m^{-2} during a shrubland fire (Morandini and Silvani 2010). Fire intensity during prescribed burns is usually much lower for ecological management purposes (see section 2.4). Nonetheless, a small-scale fire whirl formed very close to the fire fighters as seen in the photos in Fig. 6. Although no fire fighters were injured during the event due to their safe distance from the fire whirl, it should be emphasized that the potential for unpredictable fire whirl formation during low-intensity, controlled burns exists.

Near-flame plume temperatures were measured using the thermocouple array as the fire front passed the tower. Unlike the radiative heat flux that is measured from the flaming front, the observed plume temperatures (Fig. 11b) can be used to directly quantify the plume heating rates (Clements 2010) and timing of the FFP. An observed increase in the temperature at 3.5 m AGL between 12:44 and 12:46 PDT was caused by the tilted smoke plume ahead of the fire front impinging on the tower. The two lower

thermocouples indicated smaller temperature increases of 150 °C and 120 °C at 0.15 m and 1.9 m respectively, which are caused by the near-surface advection from the approaching flaming front. The observed temperature increase due to the plume is much lower than those observed by Clements (2010) during the FireFlux experiment.

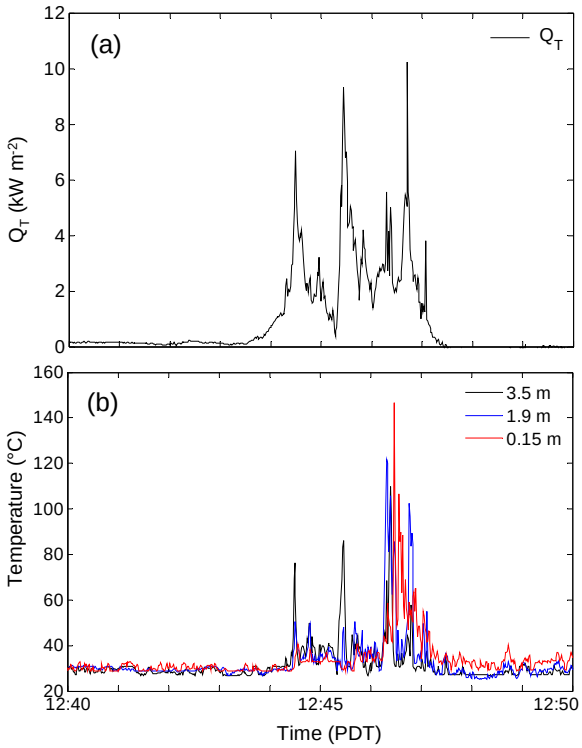

Figure 11. Time series of 1-s averaged (a) total heat flux, Q_T, and (b) thermocouple temperatures, T_c, at different levels (AGL) on the interior tower.

2.3.5 Assessment of convective Froude number

In order to determine the role fire intensity has on resulting fire behavior and the resulting atmospheric circulations, the convective Froude number is analyzed. The convective Froude number, F_c is a measure of the ratio of the kinetic energy of the air over the fire to the sensible heat flux provided by the fire (Byram 1959; Clark et al. 1996). The F_c is useful as a controlling parameter to determine the type and level of fire-

atmosphere coupling. For instance, Clark et al. (1996) hypothesized that a small F_c^2 that is indicative of strong coupling between the air and fire may be a necessary condition for a blowup fire (Byram 1954) to occur. The F_c is a non-dimensional number given by

$$F_c^2 = \frac{\left(U - S_f\right)^2}{g\frac{\langle \Delta\theta \rangle}{\langle \theta \rangle} W_f} \tag{3}$$

where U and S_f represent the wind speed and rate of spread respectively, W_f is the fire line width, θ is temperature, $\Delta\theta/\theta$ the convective buoyancy, and g acceleration due to gravity. The bracketed temperatures are the average for the period during the FFP.

The tower data and time-lapse photography allows estimating the variables necessary to calculate F_c. Prior to 12:42 PDT, when the up-valley wind was observed and the fire front was spreading against the wind, F_c was calculated using an average up-valley wind speed U_f of 2.2 m s^{-1} between 12:39 and 12:40 PDT, a forward fire spread rate S_f of 0.5 m s^{-1}, and the depth of the flaming fire front W_f of 4 m. Both S_f and W_f were estimated using the 6.7 m tower in the time lapse photos as a reference length and scaling the distances of the fire front spread over time and the depth of the flame in the photos. For instance, we used two photos to estimate that the fire front spread 6 m in 12 s from 12:40 PDT. The flame depth was estimated from a photo taken at 12:39:28 PDT (not shown). The measured thermocouple temperature profile (Fig. 11b) provides the mean temperature anomaly, $\Delta\theta$, over the fire front. A mean air temperature of the area is

obtained from the average sonic temperature. All the variables used to calculate F_c are listed in Table 1.

Table 1. Parameters used to estimate the convective Froude number during two regimes: up-valley wind (1st row) and sea breeze (2nd row). U_f represents ambient wind speed, S_f forward rate of fire spread, g gravity, θ potential temperature, $\Delta\theta$ mean perturbation temperature near the region of intense heating, W_f fire line depth, and F_c convective Froude number.

U_f (m s^{-1})	S_f (m s^{-1})	g (m s^{-2})	θ (K)	$\Delta\theta$ (K)	W_f (m)	F_C^2
2.2	0.5	9.8	301	36	4	0.61
4.1	0.75	9.8	299	36	5.5	1.73

The results show that prior to 12:42 PDT, when up-valley winds were present, F_c <1 indicating that buoyancy is the dominant mechanism and both the atmosphere and fire were essentially coupled. When the ambient wind speed increased to 4.1 m s^{-1} due to the sea breeze arrival, F_c became greater than one (Table 1). It appears F_c is less relevant to the low-level environmental shear generated by the interaction of topography and meso-scale flow and therefore, the use of F_c itself may not be suitable for predicting the fire whirl potential in this particular case. Sullivan (2007) recently re-examined the Froude number and concluded that it is not reflected in observed fire behavior, and our result is consistent with Sullivan's (2007) findings on limited usefulness of the convective Froude number for the assessment of the fire whirl potential. The large increase in TKE observed during the valley wind reversal in this study suggests that such a variable may be either used independently or could potentially be combined with F_c as a supplemental

parameter to assess whether a fire whirl is more likely. Heilman and Bian (2010) showed that the product of the Haines Index (HI) and near-surface TKE (HI×TKE) is a useful parameter to indicate whether atmospheric conditions are highly conductive to large fire development.

2.4 Summary and Conclusions

This paper presents observations made of the evolution of a small fire whirl that formed during a prescribed grass fire conducted in a narrow mountain valley. The meteorological conditions and heat release measured at a tower located in the vicinity of the fire were analyzed in an attempt to determine what caused the observed fire whirl to form. Key findings from this study include the following:

- The fire whirl occurred with the arrival of the sea breeze front in a narrow valley that was initially dominated by a daytime up-valley flow. The two opposing ambient flows produced low-level, vertical wind shear. We hypothesized that the fire whirl was caused by the interaction of the wind shear with the fire front. The fire whirl formed at the fire front and was advected behind the fire front during its evolution. The advection of the vorticity was caused by either the up-valley wind or by the formation of a pressure perturbation across the fire line.
- Estimated vorticity generated by the interaction of the wind shear and the fire front was ~0.2 s^{-1} which falls in range of magnitude simulated by Jenkins et al. (2001) during an ideal grass fire.

- The turbulence kinetic energy of the ambient wind shear (~10.4 $m^2 s^{-2}$), generated by the wind reversal, was two times greater in magnitude than turbulence generated by the buoyancy induced by the fire front. Therefore, ambient wind shear is most likely the dominant mechanism for fire whirl development in this case.
- The sensible and total heat flux measured during the fire front passage showed that the fire whirl formed during a low intensity (~12 kW m^{-2}), controlled grass fire.
- The convective Froude number, F_c was <1 when up-valley winds were present in the valley. During this time the fire was backing into the wind, buoyancy was driving the fire behavior, and the flow and fire were coupled with each other. As the wind speed increased due to the sea breeze surge, F_c became >1, which is a sign of the decreased level of the coupling. However, the convective Froude number itself may not be sufficient for fire whirl prediction because it does not take account for the near-surface turbulence generated by environmental wind shear.
- For fire management, a sudden reversal in mesoscale winds or even a diurnal, valley wind shift should be carefully monitored since the presence of two opposing flows is a favorable condition for the development of fire whirls. Although the wind shift may be brief and localized, the potential for extreme fire behavior may be high and thus should always be considered a watch out situation.

The importance of the sudden wind shift and near-surface TKE is therefore emphasized in terms of the potential for fire whirl development. Similar scenarios of wind reversals are possible in complex terrain where the valley winds transition from nocturnal drainage flows to daytime up-valley winds that can coincide with wildland fire. Additionally, further development of surface wind prediction in complex terrain (Forthofer et al. 2003) may become beneficial not only for fire spread forecasting over complex terrain but also for specifying locations prone to valley-flow convergence that can cause sudden wind shifts. The interaction of wildfires with valley-scale meteorology is not well understood and remains a topic to be investigated with both observational studies and coupled fire-atmosphere modeling systems.

Acknowledgements

This research is supported by a Joint Venture Research Agreement with the USDA Northern Research Station #07-JV-11242300-073. We thank the Cal Fire Santa Clara Unit and in particular Battalion Chief Dave McLean for conducting the prescribed burn and for accommodating our research objectives. We also acknowledge the Santa Clara County Department of Parks and Recreation for the use permit. We also want to acknowledge the stimulating discussions we had with Jason Forthofer from the USDA Forest Service FireLab in Missoula, MT and Prof. Jim Steenburgh from the University of Utah. Finally, we thank the three anonymous reviewers for their insightful comments which greatly improved the clarity and overall quality of this manuscript.

References

Atkins, N. T., R. M. Wakimoto, and T. M. Weckwerth, 1995: Observations of the sea-breeze front during CaPE. Part II: Dual-Doppler and aircraft analysis. *Mon. Wea. Rev*., **123,** 944-969.

Bluestein, H. B., C. C. Weiss and A. L. Pazmany, 2004: Doppler radar observations of dust devils in Texas. *Mon. Wea. Rev*., **132**, 209-224.

Byram, G. M., 1954: Atmospheric conditions related to blowup fires. Station Paper No. 35. USFS Southeastern Forest Experiment Station, Asheville, NC.

Byram, G. M., 1959: Combustion of forest fuels. Forest Fire: Control and Use. Eds. A. A. Brown and K. P. Davis, McGraw-Hill, N. Y., 155-182.

Clark, T. L., M. A. Jenkins, J. Coen and D. Packham, 1996: A coupled atmosphere-fire model: Role of the convective Froude Number and dynamic fingering at the fireline. *Int. J. Wildland Fire*, **6**(4), 177-190.

Clements, C. B., 2010: Thermodynamic Structure of a Grass Fire Plume. *Int. J. Wildland Fire*, **19**, 895-902.

Clements, C. B., S. Zhong, S., Goodrick, J. Li, X. Bian, B. E. Potter, W. E. Heilman, J.J. Charney, R. Perna, M. Jang, D. Lee, M. Patel, S. Street and G. Aumann, 2007: Observing the Dynamics of Wildland Grass Fires: FireFlux- A Field Validation Experiment. *Bull. Amer. Meteor. Soc.*, **88**(9), 1369-1382.

Clements, C. B., S. Zhong, X. Bian, E. Heilman, and D. Byun, 2008: First observations of turbulence generated by grass fire. *J. Geophys. Res*., **113**, D22102, doi:10.1029/2008JD010014.

Cohen, J. D., 2004: Relating flame radiation to home ignition using modeling and experimental crown fires. *Canadian J. Forest Res.*, **34**, 1616-1626, doi:10.1139/X04-049.

Countryman, C. M., 1964: Mass fires and fire behavior. U. S. Forest Service Research Paper, PSW-19, Pacific Southwest Forest and Range Experiment Station, Berkeley, CA.

Countryman, C. M., 1971: Fire whirls…why, when, and where. USFS Pacific Southwest Research Station, Berkeley, CA.

Cunningham, P., 2007: Idealized numerical simulations of the interactions between buoyant plumes and density currents. *J. Atmos. Sci*., **64**, 2105-2115.

Forthofer, J. M., B. W. Butler, K. S. Shannon, M. A. Finney, L. S. Bradshaw, and R. Stratton, 2003: Predicting surface winds in complex terrain for use in fire spread models. Proceedings of the Fifth Symposium on Fire and Forest Meteorology and Second Forest Fire Ecology and Fire Management Congress, 16-20 November 2003, Orlando, FL, 4 pages.

Forthofer, J, M. Shannon, and B. Butler, 2009: Investigating causes of large scale fire whirls using numerical simulation. Eighth Symposium on Fire and Forest Meteorology, 12-15 October 2009, Kalispell, MT, 4 pages.

Fric, T. F., and A. Roshko, 1994: Vortical structure in the wake of a transverse jet. *J. Fluid Mech*., **279**, 1-47.

Graham, H. E., 1952: A fire-whirlwind of tornadic violence. *Fire Control Note*, **13**(2), 22-24.

Graham, H. E., 1957: Fire-whirlwind formation as favored by topography and upper winds. *Fire Control Not*e, **18**(1), 20-24.

Haines, D. A. and L. J. Lyon, 1990: Horizontal roll vortices in complex terrain. *Fire Management Notes*, **51**(2), 15-17.

Hanley, D. E., P. Cunningham, and S. L. Goodrick, 2005: Interaction between a wildfire and a sea breeze front: Case study and idealized numerical simulations. *Proceedings of the EastFire Conference,* Fairfax, VA*,* 11-13 May, 2005.

Heilman, W. E., 1992: Atmospheric simulations of extreme surface heating episodes on simple hills. *Int. J. Wildland Fire*, **2**(3), 99-114.

Heilman, W. E., 1994: Simulations of buoyancy-generated horizontal roll vortices over multiple heating lines. *Forest Sci*., **40**, 601-617.

Heilman, W. E. and J. D. Fast, 1992: Simulation of horizontal roll vortex development above lines of extreme surface heating. *Int. J. Wildland Fire*, **2**(2), 55-68.

Heilman, W. E., and X. Bian, 2010: Turbulent kinetic energy during wildfires in the north central and north-eastern US. *Int. J. Wildland Fire*, **19**, 346-363.

Jenkins, M. A., T. Clark, and J. Coen, 2001: Coupling atmospheric and fire models. *Forest Fire: Behavior and Ecological Effects*, E. A. Johnson and K. Miyanishi, Eds., Academic Press, 257-302.

Jenkins, M. A., R. Sun, S. K. Krueger, J. J. Charney, and M. A. Zulauf, 2007: Effect of vertical wind shear on grassfire evolution. Seventh Symposium of Forest and Fire Meteorology, 23-27 October 2007, Bar Harbor, ME.

Meroney, R. N., 2003: Fire whirls, fire tornadoes and firestorms: physical and numerical modeling. Proceedings of PHYSMOD2003: International Workshop on Physical Modelling of Flow and Dispersion Phenomena, Prato, Italy.

Morandini, F., and X. Silvani, 2010: Experimental investigation of the physical mechanisms governing the spread of wildfires. *Int. J. Wildland Fire*, **19**, 570-582.

Pirsko, A. R., L. M. Sergius, and C. W. Hickerson, 1965: Causes and behavior of a tornadic fire-whirlwind. USFS Pacific Southwest Forest and Range Experiment Station, Berkeley, CA.

Rampanelli, G., D. Zardi, and R. Rotunno, 2004: Mechanisms of up-valley winds. *J. Atmos. Sci*., **61**, 3097-3111.

Schroeder, M. J., 1961: Down-canyon afternoon winds. *Bull. Amer. Meteor. Soc.*, **42**(8), 527-542.

Simpson, J. E., 1994: *Sea Breeze and Local Winds*. Cambridge University Press, 234 pp.

Stull, R. B., 1988: *An Introduction to Boundary Layer Meteorology*. Kluwer Academic Publisher, 666 pp.

Sullivan, A. L., 2007: Convective Froude number and Byram's energy criterion of Australian experimental grassland fires. *P. Combustion Inst.*, **31**(2), 2557-2564.

Umscheid, M. E., J. P. Monteverdi, and J. M. Davies, 2006: Photographs and analysis of an unusually large and long-lived firewhirl. *Electronic J. Severe Storms Meteor.,* **1**(2).

Whiteman, C. D., 1990: Observations of thermally developed wind systems in mountainous terrain. *Atmospheric Processes over Complex Terrain, Meteor. Monogr*., No. 45, Amer. Meteor. Soc., 5-42.

Wilczak, J. M., S. P. Oncley, and S. A. Stage, 2001: Sonic anemometer tilt correction algorithms. *Bound.-Layer Meteor*., **99**, 127-150.

Williams, N. R., 1948: Development of dust whirls and similar small scale vortices. *Bull. Amer. Meteor. Soc.*, **26**, 106-117.

CHAPTER 3

Turbulence spectra measured during fire front passage

Submitted to *Agricultural and Forest Meteorology*

Abstract

Four field experiments were conducted over various fuel and terrain to investigate turbulence generation during the passage of wildland fire fronts. The results of our spectral analysis show increased energy in velocity and temperature spectra at high frequency during fire front passage (FFP) for all four cases. However, spectral energy of velocity components at low frequencies may be affected by cross-flow intensity, topography, presence of canopy layer, and degree of fire-atmosphere coupling. When the spectra are normalized using the friction velocity u_* following Monin-Obukhov scaling, velocity spectra observed during the FFP collapsed into a fairly narrow band in the inertial subrange, suggesting that the friction velocity u_* is a valid scaling parameter that can be used for wildfire application. Temperature spectra during the FFP may not be processed properly by Fast Fourier Transform due to extreme spike in temperature values associated with the fire front passage. The scaling temperature T_* may not be an appropriate scaling parameter in extreme surface heating environment of fires as the normalized temperature spectra during the FFP does not show any systematic behaviors.

3.1 Introduction

Recent advances in numerical modeling of fire-atmosphere processes make it possible to simulate both the small-scale fire-atmosphere interactions that occur at spatial scales on the order of tens of meters at the fire front and larger-scale atmospheric forcings affecting the entire fire area that occur at spatial scales on the order of kilometers (Jenkins et al. 2001). However, few studies have focused on the observed turbulence structure in the immediate environment of propagating fires to further understand the scales of the interaction. Therefore, few principles exist from which to describe the behavior of strongly perturbed flow near the surface around the fire front. This is because conducting meteorological measurements near the fire front, even during prescribed fires, is challenging and collecting reliable data with a risk of damaging the instrumentation is a major concern. Consequently, detailed in-situ turbulence measurements have been very limited.

In-situ turbulence measurements made recently over flat terrain with grass fuel types during the FireFlux experiment (Clements et al. 2007; Clements et al. 2008) showed increases in both horizontal and vertical velocity variances at the fire front, with the largest increase in the vertical velocity variance caused by convective motion from heat flux. The turbulence spectral analysis of the vertical wind velocity, w, measured by Clements et al. (2008) revealed a general increase in the w spectral density at lower frequencies during the fire while the overall shape of the spectral density did not change in the high frequency range. The result suggests that large eddies induced by the fire may contribute to the overall turbulence generation. While the spectral analysis performed by

Clements et al. (2008) provides useful information regarding spectral energy modified by a grass fire as reference spectra, more field observations of in-situ turbulence data during fires are required for further comparisons. In addition, the spectral analysis of horizontal velocity components is necessary to fully understand the interaction of the fire with the atmosphere.

The ability to predict the rate of fire spread is one of the most important requirements for successful fire suppression, and operational fire spread rate predictions may be improved by accounting for the effect of turbulence and eddies in the ambient wind on fire spread (Sun et al. 2009). Albini (1982, 1983) attempted to combine an empirical representation for the power spectral density of horizontal wind near the ground with a theoretical model in order to predict the variability of fire spread rate and intensity of wind-aided free-burning line fires. His results suggest that free-burning line fires are responsive to wind speed variations in the frequency range below 0.1 Hz and fire intensity variations are likely to be nearly periodic at the very low frequency. Furthermore, he found the fire spread rate variability to be rather erratic, with standard deviations exceeding the mean value in many cases for timescales on the order of a minute. It should be noted, however, that power spectra of the fire spread rate and intensity in his study were derived from the wind speed at near mid-flame height in the absence of a fire on the site. Therefore, the fire-atmosphere coupling or interaction was not included. Anderson et al. (1982) showed that slight changes in the wind speed observed both upwind from the ignition point and across the path of the fire produced substantial variations in the rate of spread of a headfire. The impact of fire-induced

turbulence on the rate of spread variation could not be ruled out for the variations. Wind effects on the geometric and thermal properties of the flame front have been investigated at the field scale by Morandini et al. (2006). Their results suggest that the flame shape, temperature, and heat flux were affected by the observed large-scale wind fluctuations, and therefore they highlighted that the large-scale turbulence plays a significant role on fire spread. While their results provided useful information on the influence of wind on fire, more experiments under a wide range of wind conditions are essential to be more conclusive about the interaction between fire and turbulence.

The characteristics of the atmospheric surface layer (ASL) turbulence spectra have been studied extensively to explore whether data from different sites and heights with different stability conditions display a universal behavior in terms of Monin-Obukhov similarity relationships (Cava et al. 2001). Spectral analysis of the atmospheric turbulence, by decomposing a series of measurements into frequency components, allows for the general description of turbulence structure in terms of a few scaling parameters as power spectral density reveals how much of the variance is associated with a particular frequency. Within the framework of similarity theory, Kaimal et al. (1972) described the behavior of turbulence spectra in the surface layer over flat and homogeneous terrain using wind and temperature data collected during the Kansas experiments. It was found that all spectra reduce to a family of curves so that they converge into a single set of universal curves in the inertial subrange but diverge at lower frequencies according to the stability parameter z/L, where z is the measurement height and L the Obukhov length. In addition, it was shown that the spectra fall off with $n^{-5/3}$ in the inertial subrange, where n

represents natural frequency. Based upon the systematic behavior of the velocity and temperature spectra found by Kaimal et al. (1972) as an 'ideal' reference for flat terrain, the spectral characteristics of turbulence were studied further to test the validity of the similarity theory under non-ideal conditions.

In complex terrain, turbulence characteristics depend strongly upon changes in upwind surface roughness, and therefore it is difficult to draw firm conclusions about turbulence behavior modified by topography. Andreas (1987) showed that increased horizontal spectral energy at lower frequency is due to topography, and similar modification was also observed in the results by Al-Giboori et al. (2001). Vertical velocity spectra were observed to be less affected by the effect of topography and thus display very similar spectral properties as those over homogeneous terrain (e.g., Al-Jiboori et al. 2001; Cava et al. 2001; Panofsky et al. 1982). It should be noted that studies of turbulence spectra in complex terrain were focused primarily on hills and changing surface properties rather than in mountain valleys.

Turbulence spectra observed within plant canopies were summarized in Finnigan (2000). Liu et al. (2001) demonstrated that the maximum turbulent energy of the velocity and temperature inside the forest canopy shift toward higher frequencies as compared with previously observed spectra over flat terrain, emphasizing more contributions from smaller eddies. Their results also indicate that the normalized velocity and temperature spectra obey the -5/3 slope in the inertial subrange reasonably well, while Kaimal and Finnigan (1994) suggest a slightly steeper roll-off rate in the inertial subrange for the velocity spectra within the canopy.

The results of the spectral analysis for atmospheric motions have been used for parameterizing eddy diffusivities for air pollution problems. For example, the eddy diffusivity coefficients can be specified by using the spectral maximum frequency. The turbulent dissipation rate, estimated from the inertial subrange of the spectra, could also be used for plume rise calculations (Yadav et al. 1996). Additionally, CALPUFF (Scire et al. 2000), a default dispersion model used in BlueSky smoke modeling framework (Larkin et al. 2009) for addressing local and regional smoke impacts caused by wildland fire, includes an option to estimate the dispersion coefficients σ_v and σ_z based on similarity theory. The validity of the similarity theory, however, must be questioned when used for wildland fire applications because the perturbed boundary layer over an extremely heated surface as fire propagates is not well understood in the micrometeorological sense. One of the reasons is the lack of appropriate experimental datasets that could be used to develop a conceptual framework for describing flow and turbulence in the wildfire environment.

Our overall objectives in this research are: 1) to investigate the properties of turbulence spectra over a surface during fire front passage (FFP) as compared to those before and after FFP, which allows us to directly measure the spectral energy generated by fire-induced turbulence and, 2) to revisit the validity of the surface layer similarity theory but with effects of fire dynamics coexisting with boundary layer turbulence. Since there is no other suitable conceptual framework related to the description of turbulence spectra from the surface layer with the presence of fire, this study represents an initial attempt to evaluate the applicability of similarity law in this type of environment.

3.2 Experiments

Four field experiments were conducted in 2008-2010, each with its unique site and fire characteristics (Fig. 12). Time-series data from these four experiments are used in the subsequent analyses.

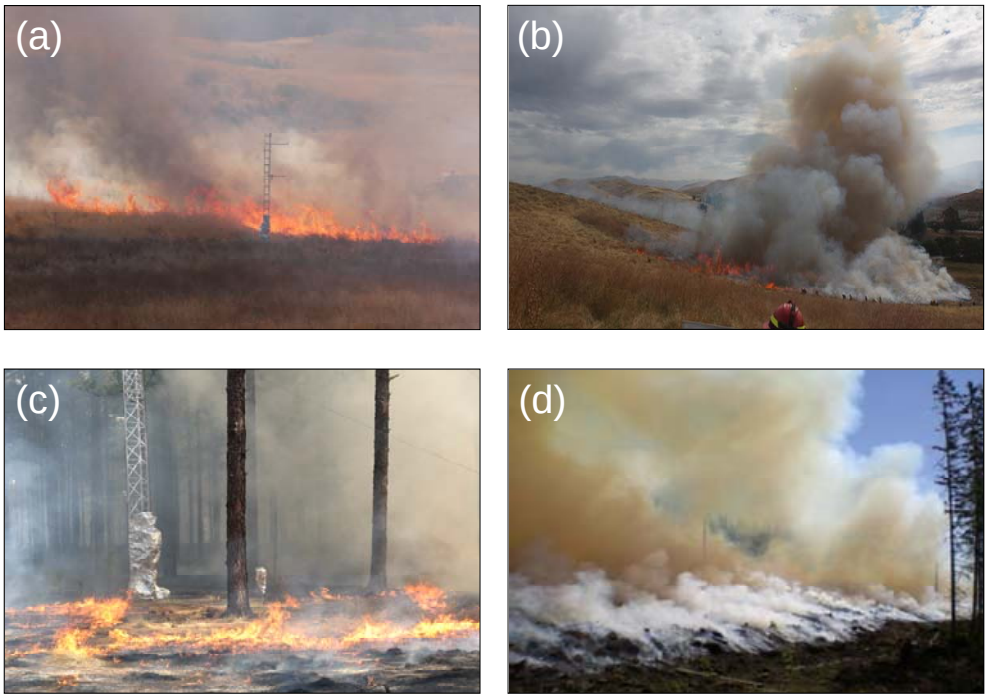

Figure 12. Photographs of fire front and instrumented flux tower within burn perimeter during (a) EXP1 at Joseph D. Grant County Park, CA; (b) EXP2 at Camp Park, CA; (c) EXP3 at Calloway Forest, NC; and (d) EXP4 at Hyytiälä, Finland. Descriptions of each experimental burn are summarized in Table 2.

3.2.1 Experiment 1: Grass fire in valley

This observational campaign was conducted during a vegetation management fire (prescribed burn) conducted by Cal Fire (California Department of Forestry and Fire Protection) on 7 October 2008 at Joseph D. Grant County Park (37° 19'N, 121° 42'W).

The park is located in the Diablo Range approximately 6.5 km east of San José, California and 60 km east of the Pacific Ocean. The experimental site is located in a northwest-southeast oriented valley, with the valley bottom elevation of 440 m above Mean Sea Level (MSL) surrounded by ridges that rise 660 m on the west and 830 m on the east. A detailed description of the site is discussed in Seto and Clements (2011). The burn unit was 0.14 km^2 (35 acres) in size, dominated by grass fuels including Italian Rye (Lolium Multiflotun), Oat Grass (Avena Barbata), Soft Brome (Bromus Hordeaceus), and Purple Needle Grass (Nassella Pulchra). The soils were dry and fuels were fully cured. The estimated fuel loading was 0.12 kg m^{-2} (0.5 tons $acre^{-1}$). To capture the micrometeorology of the passing fire front, a 6.7 m guyed, steel tower was deployed near the center of the burn unit and the fire front was allowed to burn directly underneath as a head fire (a fire that moves in the direction of the wind). Low relative humidity (25-40%) and clear skies were observed throughout the experiment.

3.2.2 Experiment 2: Grass fire on slope

The Grass Fires on Slopes Experiment was conducted on 24 June 2010 at the Camp Parks Reserve Forces Training Area (37°43'N, 121°52'W, 128 m MSL) located near Dublin, California and ~50 km north-northwest of Experiment 1 site. The primary goal of this experiment was to determine the role of fire-atmosphere interactions on fire behavior during a head fire running upslope. In-situ measurements were made with a 12 m micrometeorological tower placed in the middle of a 250 m-long, north northwest-south southeast oriented 20° slope. The hill height is approximately 50 m and several hills and ridges with similar heights are also surrounding the site. The burn unit was

approximately 0.02 km^2 (5 acres) in size, with fully cured tall grass similar to the first site mentioned above. Problems arose when the winds did not allow for upslope fire spread and therefore, the fire was ignited across the slope in a complicated ignition pattern with multiple ignition lines. The prevailing wind direction was from the west (cross slope) at 7 m s^{-1}. The upwind terrain characteristics ~4 km to the west include multiple hills with similar hill top heights. The atmospheric boundary layer during the experiment was characterized by high relative humidity (70-88%) and strong winds. Skies were mainly cloudy before the ignition due to the wide spread stratus over the area, becoming partly cloudy during the burn. Ignition started at 0900 LT and the burn was completed by 1000 LT. The instruments became inoperable ~10-min after the FFP at the tower due to the power shutdown caused by the cable damage.

3.2.3 Experiment 3: Low-intensity fire within canopy

A comprehensive field program was conducted during a prescribed sub-canopy burn in The Nature Conservancy's Calloway Forest (35° 01'N, 79° 17'W, 130 m MSL), in North Carolina during March 2010. The primary objective of the research was aimed specifically at low intensity and smoldering fire for studying smoke emissions, transport, and dispersion properties within canopies. Observational data were collected using a 23 m (75 feet) guyed, aluminum tower in a uniform ~80 year old stand of 18 to 20 m long-leaf pine (*Pinus palustris Mill.*) forest with sandy soil on relatively flat terrain. A mixture of 1-hr and 10-hr fuels of longleaf pine litter, turkey oak and wiregrass were the primary fuels on the ground in the burn unit (Unit 14) where 0.25 km^2 (61 acres) were burned with a backing fire. Ignition started at 1120 LT from the northeastern corner of the burn

unit and the flaming phase of the burn was over at 1520 LT. Low relative humidity (20% before the ignition; 13% during the burn) was observed with light wind speeds within the canopy, although moderate winds were present at the canopy top. Although the 20-m instrumented tower was deployed in a relatively open, gap-like area in the canopy to allow for the placement of guy wires, the measurements on the tower were assumed to capture the turbulence regime inside the forest vegetation layer.

3.2.4 Experiment 4: Slash burn in flat terrain

Atmospheric measurements were carried out during the IS4FIRES Experiment conducted 26 June, 2009 at Hyytiälä, Finland (Clements et al. 2009). The overall experiment objective is to develop an Integrated Monitoring and Modelling System (IS) for wildland fires (IS4FIRES). The field measurement campaign included an extensive array of gas and particulate samplers located at the SMEAR II (Station for Measuring Forest Ecosystem - Atmosphere Relations: http://www.mm.helsinki.fi/hyytiala/) site (61° 51'N 24° 17'E, 181 m MSL), augmented with additional sensors specific to this experiment. Aircraft measurements of aerosols and meteorological conditions within and downwind of the plume were also conducted. The terrain around the station is representative of the boreal coniferous forest. The 40-year old Scots pine *(Pinus sylvestris L.)* dominated stand is homogenous for about 200 m in all directions, extending to the north for about 1.2 km. The experiment was designed to have the SMEAR II towers downwind of the burn unit in order for the smoke plume to impinge on the instrument arrays. The burn unit was cut in February 2009 and was approximately 0.01 km^2 (2.5 acre) in size with a circular shape. A 12-m tree left standing in the slash within

the burn unit was used as a measurement platform. Ignition started at 0750 LT on the north side of the circular burn plot and continued in both clockwise and counter clockwise directions around the plot. The ignition was completed by 0940 LT on the southeast side of the plot. Unfortunately, turbulence data were not collected long enough after the burn to calculate the post-FFP turbulence statistics and spectra. Hereafter, we reference the Experiments 1-4 as EXP1-EXP4, respectively.

3.2.5 Instrumentation

In-situ turbulence data were measured at each of the above four sites with the same instrumentation, but at different measurement heights. All measurements were made using a 3-D sonic anemometer (Applied Technologies, Inc., Sx-probe) sampled at 10 Hz, and the instantaneous data were recorded using a Campbell Scientific, Inc. CR3000 datalogger mounted near the base of the tower housed in an environmental enclosure. In addition, an array of fine-wire thermocouples sampled at 1 Hz was used to measure plume and near-surface temperature profiles. The datalogger and the base of the tower were protected from the extreme heat generated by the fire using fireproof insulation material wrapped around the lowest 2 m of the tower. Additionally, some fire resistant sheathing was used to protect the instrument cables. Measurement heights are summarized in Table 1 along with the burn plot information.

Table 2. Summary of the experimental site, burn operation, and instrument height for the experimental burns (a)-(d) shown in Fig. 12.

	a (EXP1)	b (EXP2)	c (EXP3)	d (EXP4)
Location	CA	CA	NC	Finland
Burn date	Oct. 7, 2008	June 24, 2010	Mar. 7, 2010	June 26, 2009
Terrain	in a valley	hill	under canopy	flat
Burn size in km^2 (acres)	0.14 (35)	0.02 (5)	0.25 (61)	0.01 (2.5)
Fuel type	grass	grass	long leaf pine litter	pine timber slash
Type of burn	head	head	back	back
Instrument height (m AGL)	6.7	11	3	12

3.2.6 Data processing

The time series data of wind velocity and sonic temperature were divided into three periods: pre-, during-, and post-Fire Front Passage (FFP) data. The during-FFP block was selected first so that the center of the 30-min block (18000 data points) matched the time-series sonic temperature peak. The sonic temperature remained well above the ambient temperature over 30-min during EXP4 due to smoldering, so multiple spectral outputs were block-averaged to produce a single during-FFP spectral curve. For this study, the 30-min block size was chosen to capture both fine-scale turbulence and larger eddies generated by fire-atmosphere interactions. The same time window was applied to the velocity time series data to define during-FFP velocity data. Next, pre- and post-FFP sections were selected as before and after the during-FFP periods and limited to

daytime periods, since it has been shown that spectra under stable conditions (i.e., nighttime) are different from those under daytime convective conditions (Kaimal and Finnigan 1994). The pre- and post-FFP sections were further divided into several 30-min runs for the block averaging procedure performed later. This 30-min block-averaging has been used by several investigators (e.g., Van Gorsel et al. 2003; Zhang et al. 2010; Katurji et al. 2011) to study boundary layer turbulence structure, and it also removes the effect of the diurnal cycle and mesoscale phenomena (Nelson et al. 2007). A despiking routine was then performed to remove erroneous spikes in each 30-min block in pre- and post-FFP periods. Spikes that were four times the standard deviation were replaced by linearly interpolated values. Unrealistic spikes in the during-FFP blocks were visually inspected, removed and replaced since the FFP period is a special circumstance of high turbulence levels associated with exceptionally strong surface heating (Lee et al. 2004). The horizontal wind velocities u and v are rotated into streamwise (prevailing wind direction) and crosswise (perpendicular to streamwise direction) components, respectively, and the vertical velocity component is tilt-corrected following Wilczak et al. (2001) in order to remove any bias of the anemometer mounting not being precisely level during deployment.

Caution is needed in calculating the during-FFP velocity and temperature perturbations from the block-averaged mean values because the 30-min block containing the FFP will be characterized by a mean velocity and mean temperature that may be quite different than the mean velocity and mean temperature during 30-min periods before and after the FFP. Consequently, the computed velocity and temperature perturbations

during the FFP may not be a true reflection of the fire-induced perturbations. In this study, the during-FFP velocity and temperature perturbations were calculated from the 30-min block average mean one block prior to the during-FFP block, so that the calculated during-FFP perturbations are more representative of the fire-induced turbulence.

Wind velocity and temperature power spectra were computed using a Fast Fourier Transform (FFT) function provided in the MATLAB software. Because the raw spectral output data result in excessive crowding and numerous scatter of spectral density estimates at the high-frequency side when plotted on a log-log scale, making the expected power law in the inertial subrange difficult to see, a frequency smoothing was performed following McNaughton and Laubach (2000) to extract representative spectral curves from the excessively scattered output. The first 20 spectral coefficients were calculated using an overlapping average width (bin size) of 3 points. This process produced 18 averaged spectral estimates from the low-frequency end and is believed to reduce the most erratic variations at the statistically less reliable low-frequency side (McNaughton and Laubach 2000). Other coefficients were averaged into 39 non-overlapping bins with logarithmically increasing bin sizes so that they appear equidistant on the logarithmic frequency axis. As a result, each smoothed spectrum consists of 57 points. The individual wind velocity and temperature spectra were first normalized at the natural frequency n by the friction velocity u_* and the scaling temperature T_*, respectively, and those parameters are defined as

$$u_* = \left[\left(\overline{u'w'}\right)^2 + \left(\overline{v'w'}\right)^2\right]^{1/4} \quad (1)$$

$$T_* = -\overline{w'T'}/u_* \quad (2)$$

where *u', v', w'*, and *T'* are fluctuations of streamwise, crosswise, and vertical velocity and sonic temperature from the block-average value of the each variable, respectively. The $\overline{v'w'}$ term is included in u_* to take into account the possibility that the stress tensor may not be aligned with mean wind (Roth and Oke 1993). The normalized spectra were averaged into a single curve of the pre-, during-, and post-FFP for each burn. The frequency of each curve was normalized by *z/U*, where *z* is the measurement height and *U* is mean horizontal wind speed measured at the height *z*.

3.3 Results

3.3.1 Observed velocity variances

Variances of wind velocity indicate the physical fluctuation intensity associated with velocity perturbations from the mean (Katurji et al. 2011). The 30-min averaged variances are presented in Table 3.2. The horizontal variances during the FFP are largest during the EXP1. However, the valley wind-sea breeze reversal that occurred a few minutes before the FFP is the likely cause of these large variance values, as described in Seto and Clements (2011). Very similar observations of increased horizontal variances were also observed by Clements et al. (2008) when a dust devil developed over the burned field. Little increase in *w* variance was observed in both studies when the

horizontal variances increased. Nonetheless, increases in the horizontal variances due to the fire are expected to be intermixed with the influence of the wind shift, as the horizontal variances observed at the other three experiments consistently show higher values during the FFP.

Table 3. Values of 30-min averaged horizontal mean wind speed U (m s^{-1}), friction velocity u_* (m s^{-1}), and variances of u, v, and w (m^2 s^{-2}), and temperature (K^2) observed at each site. * indicates the mean value calculated from 1-s sampled RAWS data located at the ridge top. ** indicates the mean value calculated from 5-s sampled RAWS data located near the outside edge of the burn perimeter.

		a (EXP1)	b (EXP2)	c (EXP3)	d (EXP4)
	pre	2.33	6.86	1.05	1.06
U	during	3.33	7.21	1.78	2.58
	post	3.66	7.07*	1.05	1.51**
	pre	0.29	0.58	0.20	0.26
u_*	during	0.53	0.89	0.31	0.65
	post	0.39	——	0.22	——
	pre	0.48	1.60	0.57	0.40
σ_u^2	during	6.21	2.96	1.65	2.89
	post	1.33	——	0.53	——
	pre	0.47	0.93	0.60	0.35
σ_v^2	during	3.87	2.43	1.15	2.00
	post	1.69	——	0.69	——
	pre	0.16	0.28	0.10	0.17
σ_w^2	during	0.44	1.27	0.41	1.84
	post	0.34	——	0.10	——
	pre	0.62	0.04	0.44	0.18
σ_T^2	during	28.3	5.95	57.9	45.4
	post	0.82	——	0.28	——

Large ambient velocity variances are evident during the EXP2, due perhaps to the moderate mean flow interacting with the hilly terrain and causing the increased turbulence at the mid-slope measurement site. Despite the moderate ambient mean wind speed and the high horizontal variances, FFP caused further increases in both the horizontal and vertical variances. Of particular interest is the increase in cross-wind variance σ_v, which is aligned with the slope axis. Fire spread under cross-slope winds has been explored very little; therefore, it is difficult to explain the exact cause of the large increase in σ_v. However, the mechanical obstruction of the ridge to airflow is favorable for eddy formation on the lee side, and the flow of hot air from the fire should flow upslope, intensifying the eddy formation (Countryman 1971). Also noted is the large value of the friction velocity u_* at the site even before the burn, as compared to the near-typical values observed at the other sites. This suggests the existence of high turbulent motion near the ground at such locations under moderate flow.

All variables shown in Table 3 during EXP3 changed little before and after the FFP, showing no major turbulence development beneath the canopy during the day. However, increased mean wind velocity and variances were observed during the FFP, indicative of the development of fire-induced winds within the canopy. In contrast, a large increase in the horizontal mean wind during the FFP is evident for the EXP4 in spite of the relatively small burn area, indicative of strong fire induced winds. It is believed that the combination of a unique circular ignition pattern and very light ambient winds were favorable for convergent flow at the surface near the fire. A coupling between the atmosphere and fire can take place under the light ambient winds combined

with strong buoyancy forcing generated by higher heat intensity associated with an increased fuel loading of pine timber slash. The values of u_* and variances during FFP are rather similar in magnitude to those observed during EXP2.

The variances shown in Table 3 suggest that the fire fronts generate turbulence in both the horizontal and vertical velocity components. This is true regardless of the measurement height for all four experiments. Increased variances during the FFP were also observed by Clements et al. (2008) during the FireFlux experimental grass fire. However, it should be noted that our variances are averaged over 30 min. Variances that are calculated based on shorter averaging periods (e.g., 1-min averages used by Clements et al. (2008)) should yield higher values. Although the during-FFP variances indicate a greater increase in streamwise than crosswise directions for all cases, the increased crosswise turbulent energy is also large and may be related to the spread rate of the fire flank near the surface.

It also suggests increases in turbulence kinetic energy (TKE), $e = ½ (\sigma_u^2 + \sigma_v^2 + \sigma_w^2)$, due to both horizontal and vertical motions induced by convective motion at the fire front. The contributions of horizontal velocity variances to the TKE are greater for all cases during the FFP. The decreased degree of anisotropy in TKE is evident when the fires passed through the towers, as the ratio of the horizontal to the vertical velocity variances observed during the EXP2, EXP3, and EXP4 experiments decreased during FFP as compared to the ratios of those observed before and after the FFP (Table 3). The ratios range from 2 to 7 before and after the FFP, with the largest anisotropy found within the canopy. The values agree with observed values by Yadav et al. (1996) in unstable

conditions. Although the vertical velocity variances increased relative to the horizontal variances during the FFP, the turbulence field remained quite anisotropic within the canopy.

Overall, the turbulence statistics derived from time series velocity data show that the fire front causes an increase in variances, and the fire-induced turbulence is rather three dimensional in nature. The following sections discuss how much of the variance of a time series is associated with a particular frequency through the spectral analysis.

3.3.2 Horizontal velocity spectra

To assess spectral behavior in the surface layer during the FFP at the instrumented tower we compare it with the observed spectral behavior before and after the FFP. In order to facilitate the direct comparison of magnitudes, the velocity and temperature spectra as well as the frequency of the spectra have not been normalized for this discussion. The streamwise velocity spectra are presented in Fig. 13. All pre- and post-FFP spectra approach a straight line of -2/3 slope quite well at high frequency as suggested by Kolmogorov theory (Kolmogorov 1941), showing a property of the inertial subrange. In addition, the isotropic ratios between vertical and streamwise velocity components for EXP1-EXP4 are presented in Fig. 14. In the surface layer, eddies in the inertial subrange are isotropic and Kolmogorov's inertial subrange law requires S_w/S_u = 4/3 to be locally isotropic. The requirement is fulfilled for Figs. 14a, 14b, and 14d as the ratios approach 4/3. Within the canopy, local isotropy is generally violated (Kaimal and Finnigan 1994). The observed ratio within the canopy in our study (Fig. 14c) approaches 1 and is in good agreement with the observed value of Amiro (1990) for a pine forest,

indicating that our measurements are representative of the actual turbulence regime inside the forest vegetation layer. The during-FFP spectral curve on each burn exhibit several unique features that are not observed in the pre- and post-FFP spectra. The during-FFP spectra in Figs. 13a, 13b, and 13c contain increased energy at high frequency, while Fig. 13d shows the increased spectral energy throughout the entire frequency range. As a result of the enhanced high-frequency contribution, the behavior of the inertial subrange seems to deviate slightly from the -2/3 roll-off slope for the during-FFP spectra. Since there is no energy production or dissipation in the inertial subrange, the increased energy in this region could be produced directly by high frequency horizontal motions due to fine-scale eddies and entrainment of air generated by the fire. Wieser et al. (2001) found that the lee wakes developing downwind of an obstruction (sensor component in their case) can be resolved by sonic anemometers and they clearly appear at the high-frequency end of the velocity spectrum. Fine-scale, fire-induced eddies are likely responsible for the observed high frequency variations in the winds, similar to the effect of the wakes as observed by Wieser et al. (2001).

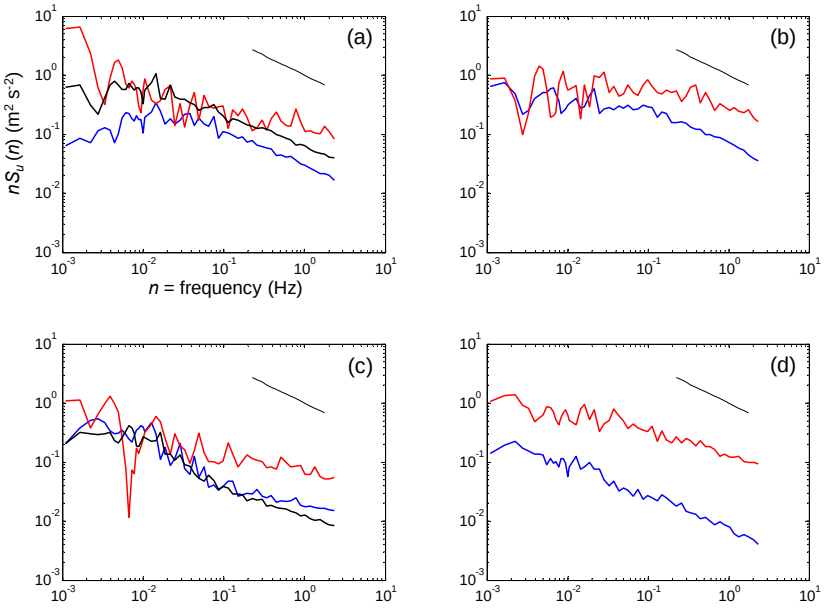

Figure 13. Non-normalized power spectra of the streamwise wind velocity $nS_u(n)$ as a function of the natural frequency n for the experimental burns (a)-(d) shown in Fig. 12. Pre-, during-, and post-FFP spectra are shown in blue, red, and black, respectively. Black straight lines indicate -2/3 slope of inertial subrange.

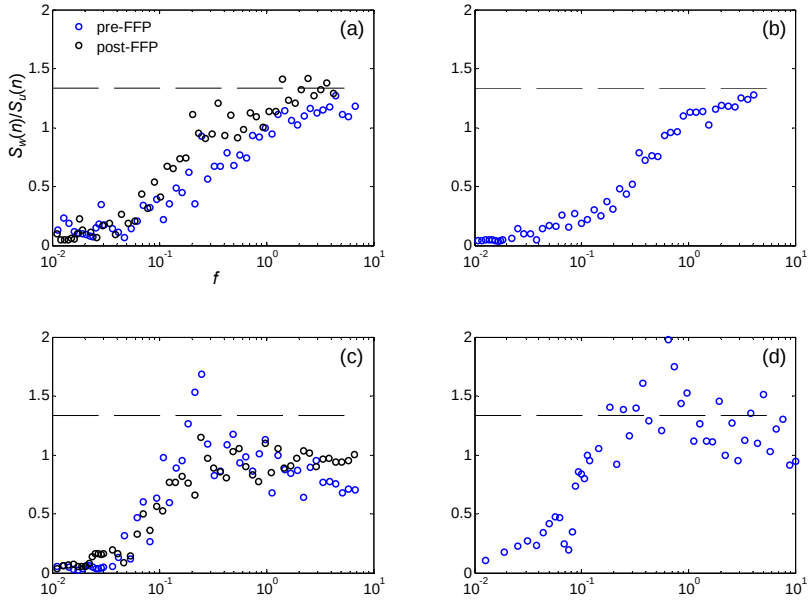

Figure 14. Ratios of vertical to streamwise power spectra as a function of the normalized frequency, $f = nz/U$ for the experimental burns (a)-(d) shown in Fig. 12. Pre- and post-FFP spectra are shown in blue and black, respectively. The ratio of 4/3 is indicated by a dashed line to allow for assessment of isotropy.

Extending the discussion further, the increased spectral energy over the inertial subrange during the FFP (as shown in Fig. 13) can be explained from the results of laboratory scale fire-wind analysis. Weckman and Strong (1996) investigated the turbulence structure of a 31-cm diameter methanol pool fire and demonstrated that the autospectral densities calculated from measured radial and axial velocities showed the spectral peaks corresponding to an eddy frequency of 2.8 Hz. In fact, the frequency of formation and departure of the outer eddies from the base of the plume, called vortex shedding, and its frequency f in Hz for the fire diameter D in meters is approximately $f = 1.5/D^{1/2}$ (Quintiere 1998). Wildfires would shed eddies at much lower frequencies than those observed in laboratory scale fires, since D is much larger than laboratory pool fires. For example, a 100-m diameter circular burning area should shed vortices with characteristic frequencies of around 0.15 Hz. But even so, this vortex shedding frequency is almost certainly constrained to above the mid-frequency range of the atmospheric turbulence. Consequently, the scales of eddies generated by fire seem to coincide with the inertial subrange of the atmospheric surface layer spectra shown in Kaimal and Finnigan (1994).

The vortex shedding frequency certainly depends upon the fire intensity that varies with time, so it should appear in a wide range of a spectrum. Although the fire front intensity, the magnitude of heat transfer, and turbulence effects involved at the laboratory scale are typically not comparable to those in the field, the vortex shedding frequency can be used to provide a range of plausible values. The turbulence spectra of laboratory-scale fires appear to have a -5/3 Kolmogorov inertial subrange slope above 1

Hz. The fire fronts passed the in-situ towers during our experimental burns as line fires; laboratory-scale experiments show that pool fires have qualitatively similar characteristics as line fires (Quintiere 1998). Based upon the assumption that the scales of eddies shed by fires depend primarily on the heat source intensity, it is proposed that fire-atmosphere coupling is necessary in order to generate larger eddies that appear below the vortex shedding frequency of the fire.

A passage of the fire front within the canopy resulted in an increased *u* velocity spectra above 0.04 Hz (Fig. 13c) and *v* velocity spectra above 0.06 Hz (Fig. 15c), while low frequency energy shows no significant increases. Thus, it is suggested that the increased horizontal variances during the FFP (Table 3) are associated with high frequency energy. This is because the turbulent energy is produced differently within the canopy than over flat and homogeneous terrain. According to Finnigan (2000), within the canopy the dominant large eddies are produced by shear at the top of the canopy due to an inviscid instability of the inflected mean velocity profile, whereas over flat, uniform terrain the bulk of the turbulent energy within the surface layer is produced by strong shear and buoyancy. Unless the mean wind profile above the canopy is affected by the fire as observed during grass fires where downward motion occurs behind the fire front bringing down higher momentum from aloft (Clements et al. 2007), the spectral energy in the energy-containing range is not expected to change. Since the sub-canopy burn was such a low intensity, it is unlikely that the fire affected the mean wind profile above the canopy.

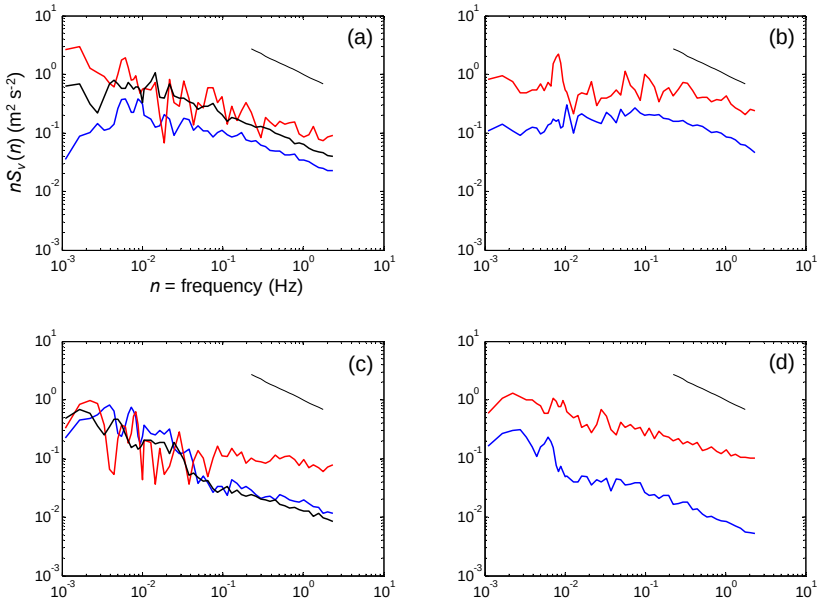

Figure 15. Same as in Figure 13, but for cross-wind velocity $nS_v(n)$.

In addition, Finnigan (2000) notes that the major contributor to momentum transfer within and just above the canopy is dominated by sweeps, the penetration of the canopy by fast, downward moving gusts. The updraft produced by the fire, in contrast, may counteract the sweeps especially above the heat source, perhaps causing the reduction of the downward momentum transfer. As a result, spectral energy at the lower frequency range in the horizontal velocity components could even decrease during the FFP as seen in the low frequency sides of Figs. 13c and 15c. The increased mean wind speed without a substantial energy increase in the energy-containing range within the canopy on the other hand, suggests that small scale turbulence perhaps influenced the mean wind profile under the canopy.

It is also noted that a marked secondary maximum in the mean wind speed was observed around $z/h = 0.12$, where h is the canopy height, within a Douglas-fir stand by

Lee and Black (1993), close to our measurement height $z/h = 0.15$. Around the height, a trunk space is relatively free of branches, allowing for less restricted air movement. Because they found that the second maximum wind speed was least coupled with the wind speed above the stand, it is hypothesized that the fire influenced the secondary maximum wind speed. Overall, the effect of the canopy combined with a low-intensity fire greatly inhibited formation of the large, energy-containing eddies and roll vortices generated by fire-atmosphere coupling (i.e., Jenkins et al. 2001).

While the primary reason for the increased spectral energy at high frequency is perhaps small eddies produced by convection and entrainment associated with the fire and plume, it is also evident that the high frequency turbulence energy was generated partly due to the low-level wind shear within the canopy as suggested by the increased mean wind speed measured at 3m AGL during the FFP (Table 3). Interactions of the high-frequency turbulent energy produced by the fire with the aerodynamic drag of the foliage are not addressed in this study. Based upon our visual observations of the enhanced foliage motions during the FFP, however, their contribution to the high frequency energy may be large as the kinetic energy of the increased mean flow within the canopy should be converted directly into fine-scale turbulence in the wakes of canopy elements (Finnigan 2000).

Clearly shown in Figs. 13d and 15d is the increased spectral energy in the horizontal velocity components over the entire frequency range during EXP4. A circular ignition pattern over the logging slash fuel under the light ambient winds led the fire behavior to a convection-driven regime near the center of the burn area, where the

instruments were located. Even though the experimental burn plot was surrounded by a boreal coniferous forest, the trees were far enough away and the clearing was sufficiently large that the turbulence characteristics were unaffected by the canopy during the fire. Thus, spectral energy within the low frequency range also increased along with the mid- and high-frequency energy. It is also hypothesized that the strong fire-atmosphere coupling resulted in the increases in the low frequency energy (large eddies) in the horizontal velocity spectra.

3.3.3 Vertical velocity spectra

All vertical velocity spectra presented in Fig. 16 show well-defined peaks in the mid-frequency range, even during the FFP when compared with the horizontal velocity spectra. In fact, the spectral peak frequencies during FFP are similar to the spectral peak frequencies before and after the FFP. All during-FFP spectra suggest that the increased vertical velocity variance presented in Table 3 was caused by the increased energy from low and high frequencies.

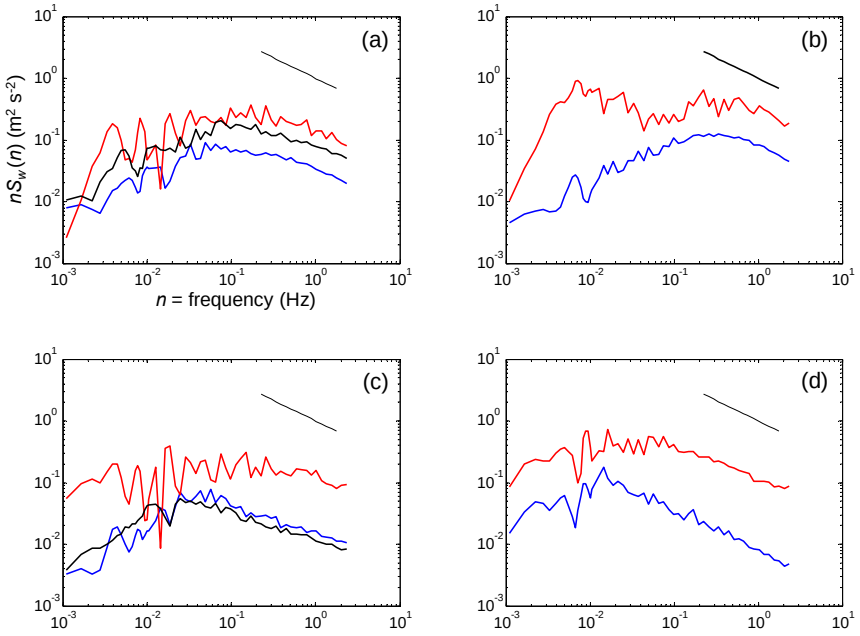

Figure 16. Same as Fig. 13, but for vertical velocity $nS_w(n)$.

The post-FFP vertical velocity spectrum for EXP1 (Fig. 16a) shows increased spectral energy at all frequencies as compared with the pre-FFP spectra. The higher post-FFP mean wind speeds are associated with a sea breeze intrusion into the valley, causing higher turbulence intensity. This feature is consistent with the horizontal velocity spectra (Figs. 13a and 15a), although the increased energy is much smaller in the vertical velocity component than the horizontal velocity components. However, the valley wind-sea breeze interaction resulted in increased variances only in the horizontal velocity components as discussed in the previous section, and the vertical velocity variance in Seto and Clements (2011) shows little change during the wind shift. Thus, the increased spectral energy associated with the convective eddies generated by the fire front is rather small, especially when compared with the post-FFP *w* spectrum.

To explain the physical processes involved, existing numerical model results are used here for qualitative comparisons. In a series of two-dimensional simulations with extreme temperatures (900K and 1500K) associated with a heating line source, Heilman and Fast (1992) showed that ambient crossflows (mean winds that flow perpendicular to the heating lines) play a significant role in the development of buoyancy-induced horizontal roll vortices above the heating source. They demonstrated that, when sufficiently strong ambient crossflow is present, the development of the updraft and downdraft are inhibited above the heating region and no horizontal vortices form. This result is consistent with the concept of the convective Froude number (Clark et al. 1996). It suggests that when kinetic energy of the air associated with horizontal winds is sufficiently strong to overcome potential energy provided by the surface heating, fire-atmosphere interactions become negligible. The model simulations with the 900K heating lines in Heilman and Fast (1992) are comparable with EXP1(Seto and Clements 2011) as the heat flux of 37 kW m^{-2} in the numerical setup is representative of the low-intensity fire of EXP1 with observed maximum total heat flux of ~12 kW m^{-2}.

In addition, the 900K heating line temperature represents the flame temperature for grass fires as Clements et al. (2007) observed the maximum fuel temperature of ~ 900K. While Seto and Clements (2011) did not observe the flame temperature during EXP1, their observed maximum thermocouple temperature, T_c, of 120°C at ~2 m AGL agrees very well with the observed T_c of Clements et al. (2007) at the same measurement height. By using the model simulation results of Heilman and Fast (1992) qualitatively, we hypothesize that the sea breeze had a strong influence in suppressing the vertical

development of the convective column, as opposed to the influence of the fire's buoyant forcing. This resulted in the relatively small increase in the *w* spectral energy during the FFP in comparison with that after the FFP.

Our *w* spectra observed during EXP2 (Fig. 16b) suggest that large-scale eddies are considerably enhanced during the FFP. The *w* spectrum during the FFP shows a prominent peak at $f = 0.007$ Hz, which did not exist before the FFP, while the spectral peak observed around 0.3 Hz before the FFP remains at the same frequency during the FFP, resulting in the two predominant peaks or double peaked *w* spectrum. The *v* velocity spectrum during the FFP (Fig. 15b) also shows a peak at 0.008 Hz, which coincides with the lower frequency peak in the *w* spectrum during the FFP. In contrast, the *u* velocity spectrum during the FFP shows increased energy toward the mid to high frequencies but not at the low frequency side. Since the *v* component of the velocity aligns with the slope axis of the local terrain, a possible explanation of the double-peaked *w* spectra is a development of a buoyancy-induced roll vortex over the slope as shown in the numerical simulation of Heilman (1992). He simulated the circulation patterns and turbulence energy fields associated with various surface heating-line locations and ambient crossflow conditions on simple two dimensional hills. While the experimental conditions are different than the numerical setup in Heilman in that the simulations are designed to provide the two dimensional (upslope/downslope velocity components with height) circulation patterns and do not include the cross-slope wind component, cross-slope winds are the prevailing wind directions during EXP2. Heilman demonstrated that

the presence of an ambient crossflow tends to reduce the magnitude and vertical extent of turbulent energy over heating lines on the leeward slope of a hill.

We hypothesize that despite the prevailing strong cross-slope flow, weak vorticity did form above the burn plot on the slope and extend several hundred meters vertically to generate large eddies as suggested by the *v* and *w* spectra. The vertical length scale during the FFP was approximated using the peak frequency and mean vertical velocity. The lower frequency peak corresponds to 100 m, twice the height of the hill. Although the simulations of cross-slope burn are not available to confirm the effects of the cross-slope flow, the flow may have similar dissipative effects on the vorticity in the cross-slope direction as it can tilt the convective column and limit the vertical extent of the vortices. That is perhaps why the increase in *u* spectral energy during the FFP is less pronounced at the low frequency in comparison with the increase in *v* spectral energy (Figs. 13b and 15b). Nonetheless, the effects of the crossflow on the development of vortices seem to be important in driving fire behavior and in limiting the vertical extent of the turbulence.

The vertical and horizontal velocity spectra during the FFP within the canopy burn (Figs 13c, 15c, and 16c) have very similar spectral behavior at high frequencies in that they show pronounced increased spectral energy with slightly slower roll-off slopes than the -2/3 inertial subrange slope that appears before and after the FFP. The increased high-frequency energy can be explained by the fact that low intensity fires such as in the sub-canopy burn tend to produce lower turbulence than large, intense fires as described in section 4.2.1. In addition, it is possible that downdrafts transport fine-scale eddies

generated by the interactions of convection and aerodynamic drag of the foliage downward into the vegetation layer, resulting in the high frequency energy enhancement. This physical process is similar to the spectral short cut described by Kaimal and Finnigan (1994) and Finnigan (2000). The aerodynamic drag of the foliage acts not only on the mean flow above the canopy but also on turbulent eddies of all scales larger than the canopy elements, causing the continual removal of energy from the eddy cascade and violating the fundamental assumption of Kolmogorov's -5/3 law for the inertial subrange. While Finnigan (2000) pointed out that sonic anemometers of 10-15 cm path length, such as the ATI Sx probe that we employed during the burn, have difficulty in resolving the dominant scales of wake kinetic energy (WKE) defined as the fine-scale wake component of TKE, the process is believed to contribute to the increased high frequency energy to some degree.

In contrast to the similarity seen in the horizontal and vertical spectral behavior at high frequencies during the FFP, the low frequency spectral behavior differ in that the *w* spectral curve during the FFP shows increased energy at low frequency, which did not occur in the horizontal velocity spectra during the FFP. One known effect of forest clearing is the air motion in the daytime that is directed towards the direction of the clearing as summarized in Lee (2000). It is possible that the clearing of branches above the tower site allowed for effective plume ventilation when the fire moved below the tower, resulting in the increased *w*-spectral energy. The convergence enhanced by both the fire and the forest clearing also explains the observed increased mean wind speed within the canopy during the FFP.

The spectral characteristics of the measured horizontal and vertical velocities during the FFP were analyzed using the traditional surface layer spectral analysis. Although we need more field data that are complete and well documented for comparisons and analysis to draw solid conclusions about the energetics of fire fronts and their interactions with boundary layer flows, our velocity spectra reveal unique turbulence structures that are modified by the thermodynamics of the fire fronts under various surface properties. Our results show good agreement with Clark et al. (1999) infrared camera imagery of convective dynamics during a prescribed crown fire. In both cases, convective motions during the fires had energy-containing eddies with spatial scales on the order of meters and time scales on the order of fractions of a second. There were also fire vortices on the scales of meters that continuously occurred at the fire front. The variations of low frequency or large scale turbulent energy and high frequency or fine-scale turbulent eddies suggest that the effects of the atmospheric boundary layer on fire behavior are quite large. Therefore, it is conceivable that turbulence certainly plays a fundamental role in the physics of fire spread.

3.3.4 Temperature spectra

Since temperature perturbations from the mean during the FFP are much larger than velocity perturbations, all temperature spectra during the FFP (Fig. 17) show clear separations from the ambient spectra. Before discussing the results of temperature spectra, a fundamental question arises. Large temperature increases and perturbations during the FFP may not be processed properly by FFT. Stull (1988) demonstrates that a spike in a time series can produce white noise, which appears as approximately equal

amplitude spectral energies across the whole range of frequencies. In order to check the performance of the FFT, we have inspected whether the sum of the spectral energies equal the biased variance of the original signal σ_T following Stull (1988). We noticed that the sum of the spectral energies for slope and sub-canopy fires (Figs 3.6b and 3.6c) during the FFP is much greater than the calculated biased variances shown in Table 3, which could be caused by amplified spectral energies across the whole range of frequencies or the white noise. Typical temperature variations in the plume above a fire show a rapid rise to a maximum temperature after the fire's onset followed by a slow fall in temperature (Clements 2010; Mercer and Weber 2001), so obtaining accurate temperature spectra during FFP is more difficult than for the velocity spectra. Even so, the sum of the spectral energies during the FFP as shown in Figs. 17a and 17d are reasonably close to the value of the calculated biased variance. Thus, limited discussions about the temperature spectra are presented in this section.

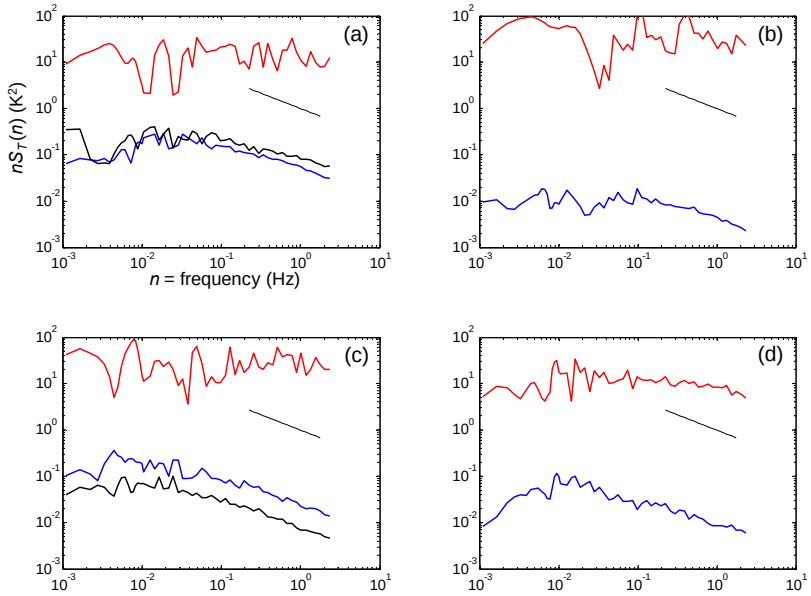

Figure 17. Same as Fig. 13, but for temperature $nS_T(n)$.

The during-FFP spectra shown in Fig. 17 lose the conventional shape of the surface layer temperature spectra shown by Kaimal et al. (1972), indicating that the temperature variations are independent from the surface layer temperature spectra within the fire environment. In addition, the characteristics of the -2/3 inertial subrange slope no longer appear at higher frequencies, and fluctuations of the spectral shape are more distinctive throughout the entire frequency range. This makes it difficult to identify the spectral peak frequency. It is suggested that during the FFP, fluctuations in both the horizontal and vertical components contribute to fluctuations in temperature because the horizontal velocity spectra show the dominant energy at the low frequency end and our vertical velocity spectra show most of the energy in the mid- to high-frequency range. It is also assumed that as the surface heating becomes strong and the convection-driven fire plume develops the influence of w on the temperature spectra increases and the influence of u decreases.

Bénech et al. (1986) presented temperature spectra observed at 25 m and 50 m above 1000 MW of artificially produced dry heat. Despite the fact that their standard deviations of the observed temperatures were much higher within the plume than in the surroundings air even at the 50 m level, their temperature spectra show a distinct spectral peak on each curve with a roll-off of energy on both sides of the peak, regardless of measurement locations and heights above and around the heat source. Their temperature spectra exhibit a faster roll-off rate of -4/3 slope through the inertial subrange than the commonly observed -2/3 slope in the surface layer. They suggest that a local modification of production-dissipation balance resulted in the departure from the standard

-2/3 slope at high frequencies and that the result is in good agreement with the observation made by Weill et al. (1976), who showed that the spectral slope of temperature fluctuation is likely to increase with the standard deviation of temperature. Their temperature measurements, however, were made using a platinum resistance thermometer that sampled at 3Hz (Bénech et al. 1986) and thermistors digitized at 30 Hz after low-pass filtering (Weill et al. 1976). As far as the overall shape of temperature spectra are concerned, our results are in qualitative agreement with the results of Rotach (1996) who showed that within the urban canyon the distribution of temperature spectral densities is almost uniform (flat). Furthermore, a random distribution of temperature fluctuations and a small roll-off at the high-frequency end were also shown. Roth and Oke (1993) suggest that the deviation from the conventional spectral curve can be related to intermittent transfer processes coupling the air within the canyon with the flow above the canyon. Similarly, our flat temperature spectra are caused by intermittent convective heat influencing the major portion of the spectral energy as compared to the temperature fluctuations driven by surface layer characteristics.

A possible reason for the two different roll-off slopes that were observed is that ultra sonic temperatures were used in both our study and Rotach (1996) for the temperature spectral analysis as compared to the thermometers and thermistors used in Bénech et al. (1986) and Weill et al. (1976). Our spectra were calculated from 10 Hz data while Rotach used 1 Hz data, and both showed similar spectral shapes. Thus, it seems that the difference in sampling rates does not contribute to the high frequency slope characteristics. Wieser et al. (2001) identified the increased roll-off slope at high

frequency and pointed out that such attenuation was caused by the fact that the instrument used was not able to resolve the high-frequency fluctuations of the wind velocity. They added that such an effect should not occur in sonic anemometer data. Thus, it is possible that thermisters and thermometers may not be able to sufficiently resolve high frequency turbulent energy produced by wakes and small eddies. This may also be true for three component propeller anemometers when compared with ultra sonic anemometers, as it is shown byYahaya and Frangi (2004) that dynamic characteristics of anemometers can result in different high frequency spectral behavior.

3.3.5 Normalized within the Monin-Obukhov similarity framework

A main advantage of normalizing spectra is to assess whether or not spectra collected under diverse conditions collapse into a universal curve particularly in the inertial subrange. Figure 18 presents the pre- and post-FFP spectra of the three velocity components and temperature for the four experiments. For clarity, the spectral densities of velocity have been multiplied by natural frequency n and normalized using u_*^2 following conventions established for Monin-Obukhov scaling. Similarly, the temperature spectra have been multiplied by natural frequency n and normalized using T_*^2. The normalized spectra are plotted against the non-dimensional frequency $f = nz/U$, where z is the measurement height, and U the horizontal mean wind speed. Without the influence of fire front passage, the velocity spectra are surprisingly well behaved in the sense that they follow the expected -2/3 slope and nearly collapsed into a narrow band in the inertial subrange, even the spectra within the canopy. The position of the velocity spectral peaks, which depends on the value of z/L presented in Table 4, seems to agree

well with the generalized spectra observed over flat terrain as shown in Kaimal and Finnigan (1994). Although no systematic spectral behavior is expected when $z/L < 0$ (unstable atmospheric conditions) for horizontal velocity spectra, our horizontal velocity spectra fall into the spectral range shown in Kaimal and Finnigan (1994). The temperature spectra behaved well in the inertial subrange as they converged into the reference temperature spectra for neutral stability obtained by Kaimal et al. (1972).

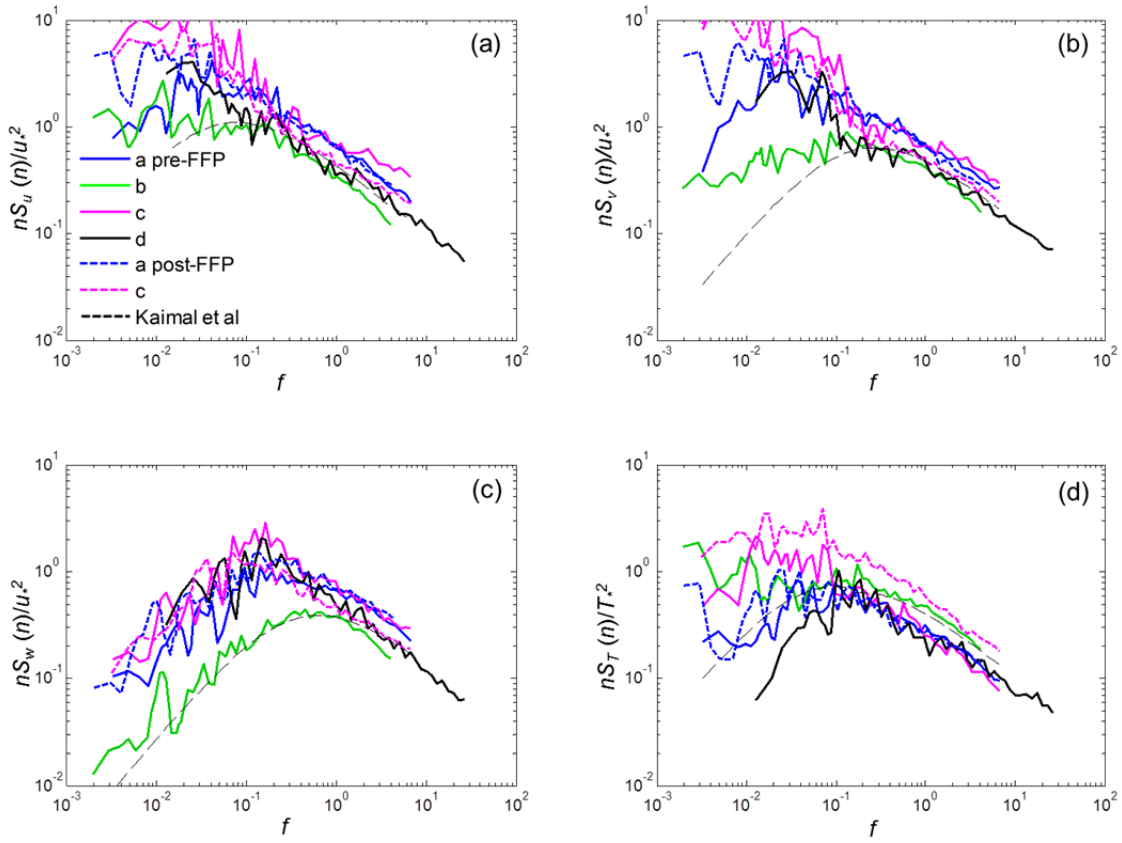

Figure 18. Normalized spectra of velocity components and temperature observed before and after the FFP during the four experiments. (a) for u; (b) for v; (c) for w; and (d) for T as a function of the normalized frequency, $f = nz/U$. The dashed lines in the plots indicate the velocity and temperature spectra for neutral stability obtained by Kaimal et al. (1972).

Table 4. Summary of the stability parameter *z/L* before, during, and after the FFP for the experimental burns (a)-(d) shown in Fig. 12.

		a (EXP1)	b (EXP2)	c (EXP3)	d (EXP4)
z/L	pre	-0.65	-0.06	-0.24	-0.99
	during	-0.56	-1.17	-3.07	-2.69
	post	-0.37	——	-0.17	——

All during-FFP velocity and temperature spectra are shown in Fig 19. All velocity spectra except for the spectrum within the canopy collapsed into a reasonably narrow range, although they exhibit greater fluctuations in the inertial subrange than those before and after the FFP in Fig. 18, due to the perturbations induced by the fires. Nonetheless, the friction velocity u_* works reasonably well as a scaling parameter for the velocity spectra during the FFP. In contrast, T_* may not be an appropriate scaling parameter as the normalized temperature spectra during the FFP does not show any systematic behaviors. This result is not surprising since the influence of the fire is so strong during the FFP that the temperature perturbations are independent of those in the surface layer. Consequently, the during-FFP spectra do not follow the reference curve obtained by Kaimal et al. (1972).

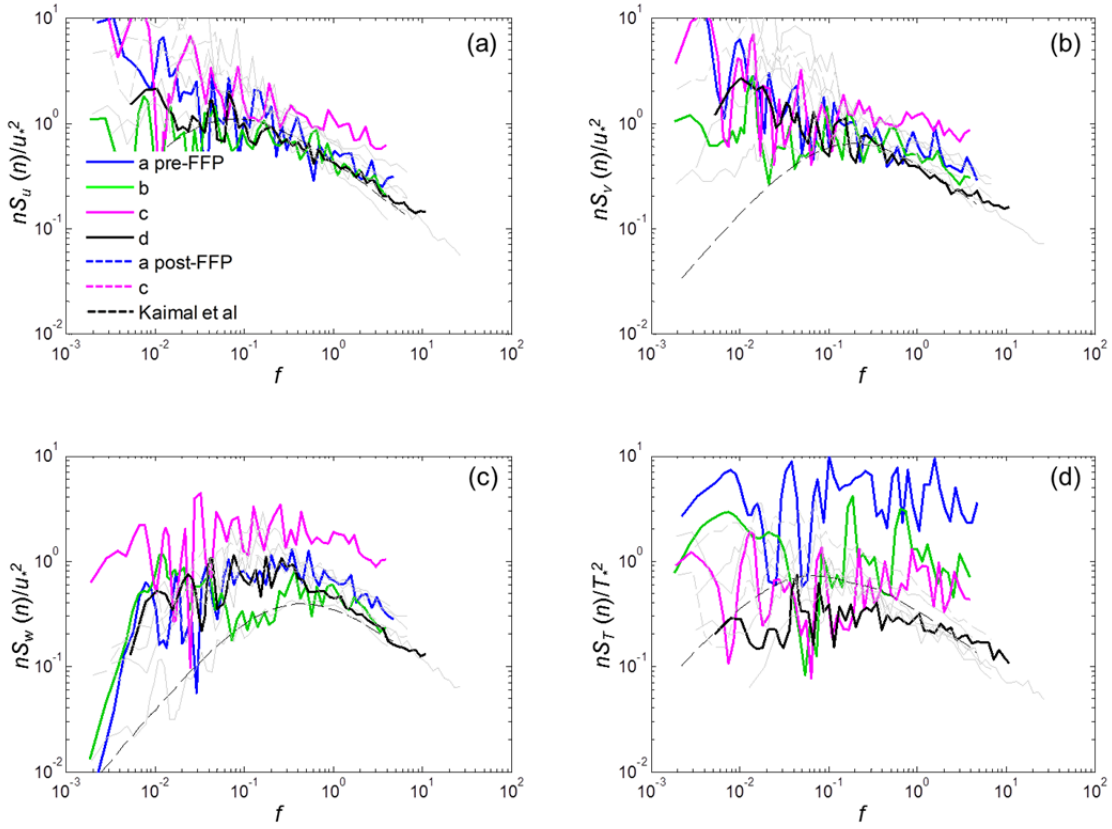

Figure 19. Same as Fig. 18 but observed during the FFP. The pre- and post-FFP spectra shown in Fig. 18 are plotted with light grey color in the background.

For the data considered, the inertial subrange of both the horizontal and the vertical spectra follow Monin-Obukhov similarity law, whereas we do not confirm a clear picture of their energy-containing regions in terms of the stability parameter. Although the results are based on limited data and include some inherent uncertainties, they show a general agreement with the results of Kaimal et al. (1972) at the inertial subrange. The incomplete understanding of turbulence generation in and around fires and their interaction with the surface layer invites further study to determine the applicability of Monin-Obukhov similarity law in fires.

3.4 Summary and Conclusions

While field validation still remains as a major difficulty in developing realistic wildfire behavior models, this research describes qualitative aspects of turbulence behavior in the very small time and spatial scales involved in the convective processes that are associated with fire front passage. The turbulence spectra in the atmospheric surface layer that was influenced by the fire's convective forcing are investigated by comparing those before, during, and after the FFP. Spectral characteristics are analyzed using existing simple numerical model results, laboratory experiments, and boundary layer concepts to identify some features that have not been adequately considered previously. Key findings from this study include the following:

- Increased horizontal mean winds and friction velocity are evident during the FFP. Turbulence intensities represented by the biased variances increased in both horizontal and vertical velocity components during the FFP for all four fire experiments.
- Our results suggest that the horizontal velocity variances have larger contributions to the TKE than the vertical velocity variance during the FFP, but a decreased degree of anisotropy in TKE was also found.
- The horizontal velocity spectra during FFP show substantial increases at high frequency for all experiments due perhaps to fine-scale eddies that are shed from the fire front, producing turbulent energy at a smaller scale than that produced by the ambient mean wind shear.

- Spectral behavior at mid to low frequency range may be affected by various environmental factors; increasing crossflow strength may inhibit the fire-atmosphere coupling and consequently, spectral energy increases little at lower frequency. Our low intensity burn conducted under the canopy (EXP3) reveals pronounced energy increases at higher frequencies, whereas low frequency energy increased little due perhaps to the fact that the fire did not affect the mean winds above the canopy layer. A slash burn (EXP4) conducted under light ambient winds exhibited increased spectral energy at all frequencies, which may have been caused by stronger fire-atmosphere coupling.
- Our vertical velocity spectra indicate substantial increases in nearly all frequencies. The strength of crossflow seems to affect the vertical velocity spectral behavior as well. The fire on the slope experiment (EXP2) that we conducted on a small hill produced a secondary *w* spectral peak at low frequency due probably to horizontal roll vortex formation.
- Our temperature spectra observed during FFP did not show the conventional spectral shape (i.e., Kaimal and Finnigan 1994). The characteristic slope of the -2/3 inertial subrange was not observed at the high frequencies, resulting in "white noise" like spectra. T_* may not be an appropriate scaling parameter as the normalized temperature spectra during the FFP does not show any systematic behaviors.
- The normalized, perturbed during-FFP velocity spectra collapsed fairly well onto a reference neutral curve of Kaimal et al. (1972) in the inertial subrange, but were

not converge closely as they were for the pre- and post-FFP. On the other hand, the normalized temperature spectra scatter randomly when scaled with T_*.

Our preliminary results show that fire can influence the energy of the flow and turbulence over a wide frequency range, and therefore the importance of the fire-atmosphere coupling in modeling physical and dynamical properties of wildfires is emphasized. While our experiments represent relatively low-intensity, controlled prescribed fires rather than intense forest fires, contributions of mean flow strength, topography, and canopy layer on turbulence intensity will be much more significant on larger and more intense wildfires. Further investigation of turbulence spectra during fire front passage is required to understand the applicability of the similarity law in wildland fires. Additionally, since many wildfires occur in complex mountainous terrain where localized wind systems already exist, those effects also need to be quantified more accurately for improved fire behavior prediction. Increased spatial density of turbulence measurements during larger experimental fires would also be beneficial to better understand the modification of fire-atmosphere interaction on large-scale surface layer flow.

Acknowledgements

All experiments were supported by a Research Joint Venture Agreement with the USDA Forest Service - Northern Research Station (#07-JV-11242300-073). The author would like to thank the Cal Fire Santa Clara Unit (and in particular Battalion Chief Dave McLean) for conducting the prescribed burn in the valley location and for

accommodating our research objectives. The Santa Clara County Department of Parks and Recreation are thanked for the special-use permit. The Contra Costa County Fire Department and other agencies involved in executing the planning and operations of the Wildfire 2010 training drill are acknowledged for accommodating our slope fire experiment. I would also like to thank Dennis Burns of the Pleasanton Fire Department for helping organize our research objectives into the burn plan. Travel support to participate in the IS4FIRES experiment is acknowledged from the Finish Meteorological Institute, and in particular, Profs. David Shultz and M. Kumala. Janne Levula is thanked for help in the installation of our instrumentation at the Hyytiälä Forestry Field Station. Dr. Tara Strand (USDA Forest Service Pacific Northwest Research Laboratory) is acknowledged for her role as PI in the sub-canopy experiments which are funded by the Joint Fire Science Program (Award # 09-1-04-2). The use of trade or firm names in this publication is for reader information and does not imply endorsement by the U.S. Department of Agriculture of any product or service.

References

Amiro, B. D., 1990: Drag coefficients and turbulence spectra within three boreal forest canopies. *Bound.-Layer Meteor*., **52**, 227-246.

Andreas, E. L., 1987: Spectral measurements in a disturbed boundary layer over snow. *J. Atmos. Sci*., **44**, 1912-1939.

Anderson, D. H., E. A. Catchpole, N. J. de Mestre, and T. Parkes., 1982: Modelling the spread of grass fires. *J. Austral. Math. Soc., (Series B)*, **23**, 451-466.

Albini, F. A., 1982: Response of free-burning fires to nonsteady wind. *Combustion Science and Technology*, **29**, 225-241.

Albini, F. A., 1983: The variability of wind-aided free-burning fires. *Combustion Science and Technology*, **31**, 303-311.

Al-Jiboori, M. H., X. Yumao, and Q. Yongfu, 2001: Turbulence characteristics over complex terrain in west China. *Bound.-Layer Meteor*., **101**, 109-126.

Bénech, B., J. Noilhan, A. Druilhet, J. M. Brustet, and C. Charpentier, 1986: Experimental study of an artificial thermal plume in the boundary layer. Part I: Flow characteristics near the heat source. *J. Climate Appl. Meteor*., **25**, 418-437.

Cava, D., U. Giostra, and M. Tagliazucca, 2001: Spectral maxima in a perturbed stable boundary layer. *Bound.-Layer Meteor*., **100**, 421-437.

Clark, T. L., M. A. Jenkins, J. Coen, and D. Packham, 1996: A coupled atmosphere-fire model: Convective feedback on fire-line dynamics. *J. Appl. Meteor.*, **35**, 875-901.

Clark T. L., L. Radke, J. Coen, and D. Middleton, 1999: Analysis of small-scale convective dynamics in a crown fire using infrared video camera imagery. *J. Appl. Meteor*., **38**, 1401-1420.

Clements, C. B., 2010: Thermodynamic structure of a grass fire plume. *Int. J. Wildland Fire*, **19**, 895-902.

Clements, C. B., S. Zhong, S. Goodrick, J. Li, X. Bian, B. E. Potter, W. E. Heilman, J. J. Charney, R. Perna, M. Jang, D. Lee, M. Patel, S. Street, and G. Aumann, 2007: Observing the Dynamics of Wildland Grass Fires: FireFlux- A Field Validation Experiment. *Bull. Amer. Meteor. Soc*., **88**(9), 1369-1382.

Clements, C. B., S. Zhong, X. Bian, W. Heilman, and D. Byun, 2008: First observations of turbulence generated by grass fire. *J. Geophys. Res*., **113**, D22102, doi:10.1029/2008JD010014.

Clements, C. B., J. Kukkonen, G. de Leeuw, A. Virkkula, J. Levula, D. M. Schultz, And M. Kulmala, 2009: An overview of atmospheric measurements made during the IS4FIRES experiments at Hyytiälä, Finland. In Eighth Symposium on Fire and Forest Meteorology, American Meteorological Society.

Countryman, C. M., 1971: Fire whirls…why, when, and where. USFS Pacific Southwest Research Station, Berkeley, CA.

Finnigan, J. J., 2000: Turbulence in plant canopies. *Annu. Rev. Fluid Mech*., **32**, 519-571.

Heilman, W. E., 1992: Atmospheric simulations of extreme surface heating episodes on simple hills. *Int. J. Wildland Fire*, **2**(3), 99-114.

Heilman, W. E. and J. D. Fast, 1992: Simulations of horizontal roll vortex development above lines of extreme surface heating. *Int. J. Wildland Fire*, **2**(2), 55-68.

Jenkins, M. A., T. Clark, and J. Coen, 2001: Coupling atmospheric and fire models, in: Johnson, E.A., Miyanishi, K. (Eds.), Forest fire: Behavior and ecological effects. Academic Press, pp. 257-302.

Kaimal, J. C., J. C. Wyngaard, Y. Izumi, and O. R. Coté, 1972: Spectral characteristics of surface-layer turbulence. *Quart. J. Roy. Meteor. Soc*., **98**, 563-589.

Kaimal, J. C. and J. J. Finnigan, 1994: Atmospheric Boundary Layer Flows. Oxford University Press, New York.

Katurji, M., A. Sturman, and P. Zawar-Reza, 2011: An investigation into ridge-top turbulence characteristics during neutral and weakly stable conditions: velocity spectra and isotropy. *Bound.-Layer Meteor*., **139**, 143-160.

Kolmogorov, A. N., 1941: The local structure of turbulence in incompressible viscous fluid for very large Reynolds numbers. Dokl Akad Nauk SSSR, **30**, 299-303.

Larkin, N. K., S. M. O'Neill, R. Solomon, S. Raffuse, T. Strand, D. C. Sullivan, C. Krull, M. Rorig, J. L. Peterson, and S. A. Ferguson, 2009: The BlueSky smoke modeling framework. *Int. J. Wildland Fire*, **18**, 906-920.

Lee, X., 2000: Air motion within and above forest vegetation in non-ideal conditions. *Forest Ecol. Manag*., **135**, 3-18.

Lee, X. and T. A. Black, 1993: Atmospheric turbulence within and above a Douglas-fir stand. Part 1: Statistical properties of the velocity field. *Bound.-Layer Meteor*., **64**, 149-174.

Lee, X., W. Massman, and B. Law, 2004: Handbook of micrometeorology. Kluwer Academic Publishers, Dordrecht, pp. 250.

Liu, S., H. Liu, M. Xu, M. Y. Leclerc, T. Zhu, C. Jin, Z. Hong, J. Li, and H. Liu, 2001: Turbulence spectra and dissipation rates above and within a forest canopy. *Bound.-Layer Meteor*., **98**, 83-102.

McNaughton, K. G. and J. Laubach, 2000: Power spectra and cospectra for wind and scalars in a disturbed surface layer at the base of an advective inversion. *Bound.-Layer Meteor*., **96**, 143-185.

Mercer, G. N. and R. O. Weber, 2001: Fire plumes. in: Johnson, E.A., Miyanishi, K. (Eds.), Forest fire: Behavior and ecological effects. Academic Press, pp. 225-355.

Morandini, F., X. Silvani, L. Rossi, P. Santoni, A. Simeoni, J. Balbi, J. L. Rossi, and T. Marcelli, 2006: Fire spread experiment across Mediterranean shrub: Influence of wind on flame front properties. *Fire Safety Journal*, **41**, 229-235.

Nelson, M. A., E. R. Pardyjak, J. C. Klewicki, and M. J. Brown, 2007: Properties of the wind field within the Oklahoma City Park Avenue street canyon. Part II: Spectra, co-spectra and quadrant analyses. *J. Appl. Meteor. Climatol.,* **46**(12), 2055–2073.

Panofsky, H. A., D. Larko, R. Lipschutz, G. Stone, E. F. Bradley, A. J. Bowen, and J. Højstrup, 1982: Spectra of velocity components over complex terrain. *Quart. J. Roy. Meteor. Soc.,* **108**, 215-230.

Quintiere, J. G., 1998: Principles of Fire Behavior. Delmar Publishers, 258 pp.

Rotach, M. W., 1995: Profiles of turbulence statistics in and above an urban street canyon. *Atmos. Environ.,* **29**(13), 1473-1486.

Roth, M. and T. R. Oke, 1993: Turbulent transfer relationships over suburban surface. Part I: Spectral characteristics. *Quart. J. Roy. Meteor. Soc.,* **119**, 1071-1104.

Scire J. G., D. G. Strimaitis, and R. J. Yamartino, 2000: A User's Guide for the CALPUFF Dispersion Model (version 5). Earth Tech Inc. Concord, MA.

Seto, D. and C. B. Clements, 2011: Fire whirl evolution observed during a valley wind-sea breeze reversal. *Journal of Combustion*, Article ID 569475, doi:10.1155/2011/569475.

Stull, R. B., 1988: An Introduction to Boundary Layer Meteorology. Kluwer Academic Publisher, Dordrecht, 666 pp.

Sun, R., S. K. Krueger, M. A. Jenkins, M. A. Zulauf, and J. J. Charney, 2009: The importance of fire-atmosphere coupling and boundary-layer turbulence to wildfire spread. *Int. J. Wildland Fire*, **18**, 50-60.

Van Gorsel, E., A. Christen, C. Feigenwinter, E. Parlow, and R. Vogt, 2003: Daytime turbulence statistics above a steep forested slope. *Bound.-Layer Meteor*., **109**, 311-329.

Weckman, E. J. and A. B. Strong, 1996: Experimental investigation of the turbulence structure of medium-scale methanol pool fires. *Combustion and Flame*, **105**, 245-266.

Weill, A., M. Aubry, F. Baudin, and J. Heissat, 1976: A study of temperature fluctuations in the atmospheric boundary layer. *Bound.-Layer Meteor*., **10**, 337-346.

Wieser, A., F. Fiedler, and U. Corsmeier, 2001: The influence of the sensor design on wind measurements with sonic anemometer systems. *J. Atmos. Oceanic Technol*., **18**, 1585-1608.

Wilczak, J. M., S. P. Oncley, and S. A. Stage, 2001: Sonic anemometer tilt correction algorithms. *Bound.-Layer Meteor*., **99**, 127-150.

Yadav, A. K., S. Raman, and M. Sharan, 1996: Surface layer turbulence spectra and dissipation rates during low winds in tropics. *Bound.-Layer Meteor*., **79**, 205-223.

Yahaya, S. and J. P. Frangi, 2004: Cup anemometer response to the wind Turbulence — measurement of the horizontal wind variance. *Annales Geophysicae*., **22**, 3363-3374.

Zhang, Y., H. Liu, T. Foken, Q. L. Williams, A. Liu, M. Mauder, and C. Liebethal, 2010: Turbulence spectra and cospectra under the influence of large eddies in the Energy Balance EXperiment (EBEX). *Bound.-Layer Meteor*., **136**, 235-251.

CHAPTER 4

Summary and Future Work

4.1 Summary

This thesis provides unique observations and analysis of fire-atmosphere interactions based on in-situ measurements during experimental fires. A fire whirl formation that occurred during a valley wind-sea breeze reversal is discussed in Chapter 2. The study presents the unique observational dataset available for eventual evaluations of fire behavior modeling with a similar vertical wind profile. It is hypothesized that the fire whirl was caused by the interaction of the wind shear with the fire front. Estimated vorticity of 0.2 s^{-1} and turbulence kinetic energy of 10.4 $m^2 s^{-2}$ were found during the interaction. The convective Froude number represents the degree of fire-atmosphere coupling well and may be combined with other parameters for predicting fire whirl potential. This study also provides useful information for fire managers, as they need to avoid burn operations in any situations that are conductive to extreme fire behavior, such as a sudden wind reversal in a valley.

Also attempted in this thesis was to describe some qualitative aspects of turbulence behavior in the very small time and spatial scales involved in the convective processes associated with FFP. The data collected from four field experiments were compared with existing model results, laboratory experiments, and boundary layer concepts to identify spectral characteristics of surface layer turbulence during fire front passage. Results from the spectral analysis performed in this study revealed increased velocity spectral energy at high frequency during FFP for all four experiments due to

fine-scale eddies shed from the fire. However, the spectral energy at lower frequencies may be affected by the degree of fire-atmosphere coupling and environmental factors such as topography and the presence of canopy layer. This study, as an initial attempt, also presents the applicability of the Monin-Obukhov similarity theory during FFP since there is no other suitable conceptual framework related to the description of turbulence spectra with the presence of fire. The normalized velocity spectra collapsed into a narrow range at high frequency even during FFP and thus, the similarity scaling works appropriately. The temperature spectra, however, did not show any systematic spectral behavior due to scaling invalidity.

4.2 Future work

Future research is planned to further investigate the fire-atmosphere interactions in complex terrain. Instrumentation includes multiple in-situ platforms with sonic anemometers and a use of the remote-sensing systems such as a Doppler lidar, a sodar, and a microwave profiler. While our spectral analysis using the high-sampling turbulence data measured in-situ captured a secondary vertical velocity peak that developed during FFP over a sloped terrain, which is also seen in a model simulation of Heilman (1992), the remote-sensing measurements allow for direct detection of the fire-atmosphere circulations that will make the results of our preliminary spectral analysis more conclusive.

Our results indicate a distinctive spectral behavior that developed during FFP within the canopy. However, measurements of the turbulence above the canopy layer are

desirable to draw a solid conclusion about the interaction between fire, atmosphere, and forest canopy. Datasets from several sub-canopy burns may be available for further analysis and comparisons.

Because developing and validating new-generation coupled fire-atmosphere models require better understanding of the complex interactions of fire, weather, atmosphere, topography, and fuels in the field, integrated field experiments are desirable. As in-situ micrometeorological observations of fire-atmosphere interactions provide information that cannot be obtained from laboratory experiments, it will remain an essential part of wildfire research. Data acquisition strategies should be continuously explored to provide clear pictures of fire-atmosphere interactions needed for model validations.

References

Banta, R. M., L. D. Olivier, E. T. Holloway, R. A. Kropfli, B. W. Bartram, R. E. Cupp, and M. J. Post, 1992: Smoke-column observations from two forest fires using Doppler lidar and Doppler radar. *J. Appl. Meteor.* **31**, 1328-1349.

Bowman, D. M. J. S., J. K. Balch, P. Artaxo, W. J. Bond, J. M. Carlson, M. A. Cochrane, C. M. D'Antonio, R. S. DeFries, J. C. Doyle, S. P. Harrison, F. H. Johnston, J. E. Keeley, M. A. Krawchuk, C. A. Kull, J. B. Marston, M. A. Moritz, I. C. Prentice, C. I. Roos, A. C. Scott, T. W. Swetnam, G. R. van der Werf, and S. J. Pyne, 2009: Fire in the Earth System. *Science*, **324**, 481-484.

Butler, B. W., J. Cohen, D. J. Latham, R. D. Schuette, P. Sopko, K. S. Shannon, D. Jiminez, and J. S. Bradshaw, 2004: Measurement of radiant emissive power and temperatures in crown fires. *Can. J. For. Res.*, *34*, 1577-1587.

Byram, G. M., 1959: Combustion of forest fuels. Forest Fire: Control and Use. Eds. A. A. Brown and K. P. Davis, McGraw-Hill, N. Y., 155-182.

Clark, T. L., M. A. Jenkins, J. Coen and D. Packham, 1996a: A coupled atmosphere- fire model: Role of the convective Froude Number and dynamic fingering at the fireline. *Int. J. Wildland Fire*, **6**(4), 177-190.

Clark, T. L., M. A. Jenkins, J. Coen and D. Packham, 1996b: A coupled atmosphere-fire model: Convective feedback on fire-line dynamics. *J. Appl. Meteor.*, **35**, 875-901.

Clark T. L., L. Radke, J. Coen, and D. Middleton, 1999: Analysis of small-scale convective dynamics in a crown fire using infrared video camera imagery. *J. Appl. Meteor.*, **38**, 1401-1420.

Clements, C. B., 2010: Thermodynamic structure of a grass fire plume. *Int. J. Wildland Fire*, **19**, 895-902.

Clements, C. B., B. E. Potter, and S. Zhong, 2006: *In situ* measurements of water vapor, heat, and CO_2 fluxes within a prescribed grass fire. *Int. J. Wildland Fire*, **15**, 299-306.

Clements, C. B., S. Zhong, S., Goodrick, J. Li, X. Bian, B.E. Potter, W. E. Heilman, J.J. Charney, R. Perna, M. Jang, D. Lee, M. Patel, S. Street and G. Aumann, 2007: Observing the Dynamics of Wildland Grass Fires: FireFlux- A Field Validation Experiment. *Bull. Amer. Meteor. Soc.*, **88**(9), 1369-1382.

Clements, C. B., S. Zhong, X. Bian, E. Heilman, and D. Byun, 2008: First observations of turbulence generated by grass fire. *J. Geophys. Res*., **113**, D22102, doi:10.1029/2008JD010014.

Clements, C. B., J. Kukkonen, G. de Leeuw, A. Virkkula, J. Levula, D. M. Schultz, and M. Kulmala, 2009: An overview of atmospheric measurements made during the IS4FIRES experiments at Hyytiälä, Finland. Poster, *8th Symposium on Fire and Forest Meteorology*, Kalispell, MT, Amer. Meteror, Soc., P1.19.

Coen, J. L., 2005: Simulation of the Big Elk Fire using coupled atmosphere-fire modeling. *Int. J. Wildland Fire*, **14**, 49-59.

Cohen, J. D., 2004: Relating flame radiation to home ignition using modeling and experimental crown fires. *Can. J. For. Res.*, **34**, 1616-1626, doi:10.1139/X04-049.

Dupuy, J. L., R. R. Linn, V. Konovalov, F. Pimont, J. A. Vega, and E. Jiménez, 2011: Exploring three-dimensional coupled fire-atmosphere interactions downwind of wind-driven surface fires and their influence on backfires using HIGRAD-FIRETEC model. . *Int. J. Wildland Fire*, **20**, 734-750.

Filippi, J. B., F. Bosseur, X. Pialat, P. A. Santoni, S. Strada, and C. Mari, 2011: Simulation of coupled fire/atmosphere interaction with the MesoNH-ForeFire models. *Journal of Combustion*, Article ID 540390, doi: 10.1155/2011/540390.

Heilman, W. E., 1992: Atmospheric simulations of extreme surface heating episodes on simple hills. *Int. J. Wildland Fire*, **2**(3), 99-114.

Jenkins, M. A., T. Clark, and J. Coen, 2001: Coupling atmospheric and fire models. *Forest Fire: Behavior and ecological Effects*, E. A. Johnson and K. Miyanishi, Eds., Academic Press, 257-302.

Kiefer, M. T., M. D. Parker, and J. J. Charney, 2009: Regimes of dry convection above wildfires: Idealized numerical simulations and dimensional analysis. *J. Atmos. Sci*., **66**, 806-835.

Linn, R. R. and P. Cunningham, 2005: Numerical simulations of grass fires using a coupled atmosphere-fire model: Basic fire behavior and dependence on wind speed. *J. Geophys. Res*., **110**, D13107, doi:10.1029/2004JD005597.

Linn, R. R., J. M. Canfield, P. Cunningham, C. Edminster, J.-L. Dupuy, and F. Pimont, 2012: Using periodic line fires to gain a new perspective on multi-dimensional aspects of forward fire spread. *Agric. For. Meteor*., **157**, 60-76.

Morandini, F., X. Silvani, L. Rossi, P. Santoni, A. Simeoni, J. Balbi, J. L. Rossi, and T. Marcelli, 2006: Fire spread experiment across Mediterranean shrub: Influence of wind on flame front properties. *Fire Safety Journal*, **41**, 229-235.

Morandini, F., and X. Silvani, 2010: Experimental investigation of the physical mechanisms governing the spread of wildfires. *Int. J. Wildland Fire*, **19**, 570-582.

Running, S. W., 2006: Is global warming causing more, larger wildfires? *Science*, **313**, 927-928.

Santoni, P. A., A. Simeoni, J. L. Rossi, F. Bosseur, F. Morandini, X. Silvani, J. H. Balbi, D. Cancellieri and L. Rossi, 2006: Instrumentation of wildland fire: Characterisation of a fire spreading through a Mediterranean shrub. *Fire Safety Journal*, **41**, 171-184.

Silvani, X. and F. Morandini, 2009: Fire spread experiments in the field: Temperature and heat flux measurements. *Fire Safety Journal*, **44**, 279-285.

Sullivan, A. L., 2007: Convective Froude number and Byram's energy criterion of Australian experimental grassland fires. *P. Combustion Inst.*, **31**(2), 2557-2564.

Sun, R., S. K. Krueger, M. A. Jenkins, M. A. Zulauf, and J. J. Charney, 2009: The importance of fire-atmosphere coupling and boundary-layer turbulence to wildfire spread. *Int. J. Wildland Fire*, **18**, 50-60.

Werth, P. A., 2011: Critical fire weather patterns. *Synthesis of knowledge of extreme fire behavior*, **1**, 25-48.

Westerling, A. L., H. G. Hidalgo, D. R. Cayan, and T. W. Swetnam, 2006: Warming and earlier spring increase western U. S. forest wildfire activity. *Science*, **313**, 940-943.